New Parameterizations of Turbulence Statistics for the Atmospheric Surface Layer

TEMPLE R. LEE[a] AND TILDEN P. MEYERS[a]

[a] *NOAA/Air Resources Laboratory Atmospheric Turbulence and Diffusion Division, Oak Ridge, Tennessee*

(Manuscript received 11 March 2022, in final form 20 July 2022)

ABSTRACT: Recent work has shown that bulk-Richardson (Ri_b) parameterizations for friction velocity, sensible heat flux, and latent heat flux have similar, and in some instances better, performance than long-standing parameterizations from Monin–Obukhov similarity theory (MOST). In this work, we expanded upon new Ri_b parameterizations and developed parameterizations of turbulence statistics, i.e., standard deviations in the 30-min u (horizontal), v (meridional), and w (vertical) wind components (i.e., σ_u, σ_v, and σ_w, respectively), which allowed us to derive Ri_b-based parameterizations of turbulent kinetic energy (e), and standard deviations in the 30-min temperature and moisture measurements (σ_θ and σ_q, respectively). We used datasets from three 10-m micrometeorological towers installed during the Land Atmosphere Feedback Experiment (LAFE) conducted in Oklahoma from 1 to 31 August 2017 and evaluated the new parameterizations by comparing them against parameterizations from MOST. We used the LAFE datasets and fully independent datasets obtained from two micrometeorological towers installed in Alabama between February 2016 and April 2017 to evaluate the performance of the parameterizations. Based on the slope of the relationship between the observed and parameterized turbulence statistics (m_b) and the coefficient of correlation (r), we found that the Ri_b relationships generally performed better than MOST at parameterizing σ_v, σ_w, σ_θ, and σ_q, and the Ri_b relationships performed better at low wind speeds than at high wind speeds. These results, coupled with recent developments of Ri_b parameterizations for surface-layer momentum, heat, and moisture fluxes, provide further evidence to consider using Ri_b-based parameterizations in weather forecasting models.

SIGNIFICANCE STATEMENT: Deficiencies in Monin–Obukhov similarity theory (MOST) are well known, yet MOST forms the basis in weather forecasting models for describing heat, moisture, and momentum transfer between the land surface and atmosphere. We expanded upon previous work suggesting a MOST alternative called the bulk-Richardson approach. We used data collected from meteorological towers installed in Oklahoma and compared the bulk-Richardson approach with MOST. We evaluated these two approaches using data from meteorological towers installed in Oklahoma and Alabama and found that, overall, the bulk-Richardson approach performed better than MOST in determining the 30-min variability in temperature, moisture, and wind. This result provides additional motivation to use a bulk-Richardson approach in weather forecasting models because doing so will likely yield improved forecasts.

KEYWORDS: Surface layer; Turbulence; Parameterization

1. Background

For more than 50 years, Monin–Obukhov similarity theory (MOST) has been used to quantify near-surface exchanges of heat, moisture, and momentum in numerical weather prediction (NWP) models. MOST expresses gradients in surface-layer wind, temperature, and moisture fields as a function of a dimensionless stability length ζ, defined as

$$\zeta = \frac{z - d}{L}. \tag{1}$$

In Eq. (1), d is the displacement height of the vegetation, z is the sampling height, and L is the Monin–Obukhov length scale defined as

$$L = -\frac{\overline{\theta}_v u_*^3}{\kappa g \overline{w'\theta'_v}}. \tag{2}$$

In Eq. (2), θ_v is the virtual potential temperature, u_* is the friction velocity, κ is the Von Kármán constant, g is the gravitational acceleration, and $\overline{w'\theta'_v}$ is the kinematic heat flux.

MOST is also used as the basis for scaling surface-layer turbulence quantities. Many different scaling relationships have been proposed that nondimensionalize the standard deviations in the wind components by dividing these quantities by u_* and then relating the nondimensionalized forms to ζ. In general, under unstable conditions (i.e., when $\zeta < 0$), these relationships are nonlinear and have the following form that has been suggested in many previous studies (e.g., Panofsky and McCormick 1960; Panofsky et al. 1977; Panofsky and Dutton 1984; Wilson 2008; de Franceschi et al. 2009; Srivastava et al. 2020):

$$\frac{\sigma_{u,v,w}}{u_*} = \alpha_{\sigma_{u,v,w}}(1 - \beta_{\sigma_{u,v,w}}\zeta)^{1/3}. \tag{3}$$

In Eq. (3), σ_u, σ_v, and σ_w are the standard deviations in the u (i.e., horizontal), v (i.e., meridional), and w (i.e., vertical) wind components; and $\alpha_{\sigma_{u,v,w}}$ and $\beta_{\sigma_{u,v,w}}$ are empirically determined fitting coefficients. Under nearly neutral atmospheric regimes (i.e., when $\zeta \approx 0$), values for σ_u/u_* have been reported to range from 1.9 to 4.5, whereas values for σ_u/u_* and σ_w/u_* can range from 1.6 to 3.8 and from 1.1 to 1.5, respectively (e.g., de Franceschi et al. 2009).

Corresponding author: Temple R. Lee, temple.lee@noaa.gov

DOI: 10.1175/MWR-D-22-0071.1

Under stable conditions (i.e., when $\zeta > 0$), there have been different functional forms that have been proposed for the relationship between $\sigma_{u,v,w}/u_*$ and ζ. For example, Al-Jiboori et al. (2002), de Franceschi et al. (2009), Quan and Hu (2009), and Srivastava et al. (2020) proposed that this relationship has the following form, again where $\alpha_{\sigma_{u,v,w}}$ and $\beta_{\sigma_{u,v,w}}$ are empirically determined fitting coefficients but only for stable atmospheric regimes:

$$\frac{\sigma_{u,v,w}}{u_*} = \alpha_{\sigma_{u,v,w}}(1 + \beta_{\sigma_{u,v,w}}\zeta)^{1/3}. \quad (4)$$

In contrast, other studies (e.g., Pahlow et al. 2001) have reported the following relationship when $\zeta > 0$ (where $\gamma_{\sigma_{u,v,w}}$ is an empirically determined fitting coefficient):

$$\frac{\sigma_{u,v,w}}{u_*} = \alpha_{\sigma_{u,v,w}} + \beta_{\sigma_{u,v,w}}\zeta^{\gamma_{\sigma_{u,v,w}}}. \quad (5)$$

There also remains no consensus on the forms of the relationship between the nondimensionalized forms of the standard deviation in temperature or moisture, i.e., σ_θ/θ_* and σ_q/q_*, respectively; and ζ. Andreas et al. (1998) reported that $\sigma_\theta/\theta_* = 3.2(1 - 28.4\zeta)^{-1/3}$ and $\sigma_\theta/\theta_* = 3.2$ when $\zeta < 0$ and $\zeta > 0$, respectively; Quan and Hu (2009) reported that $\sigma_\theta/\theta_* = -1.5(-\zeta)^{-1/3}$ and $\sigma_\theta/\theta_* = 3.0(\zeta)^{-1/3}$ when $\zeta < 0$ and $\zeta > 0$, respectively. Ramana et al. (2004) found that $\sigma_\theta/\theta_* = 6.56(1 - 9.5\zeta)^{-1/3}$ and $\sigma_\theta/\theta_* = 6.45(1 + 0.25\zeta)^{-1}$ when $\zeta < 0$ and $\zeta > 0$, respectively. In instances when $\zeta < 0$, Quan and Hu (2009) reported that $\sigma_q/q_* = 1.07(1 - 2.71\zeta)^{-1/3}$ but did not find a similarity relationship for stable conditions, noting that MOST could not adequately represent water vapor fluctuations.

In addition to a lack of consensus on the functional forms of the relationships between $\sigma_{u,v,w}/u_*$ and ζ, as well as between σ_θ/θ_* and ζ and between σ_q/q_* and ζ, there are other caveats to MOST that include e.g., 1) the assumption of a homongenous flux layer near the surface (e.g., Businger et al. 1971; Foken 2006), 2) statistical self correlation (e.g., Hicks 1978, 1981, 1995), and 3) being poorly suited for stratified surface layers (e.g., Sun et al. 2020). Thus, there remains a strong need to revise MOST (e.g., Wilson 2008). To this end, researchers have investigated the utility of the Richardson number, Ri, instead of ζ as a scaling variable (e.g., Sorbjan 2006; Mauritsen et al. 2007; Sorbjan 2010, 2017; Greene et al. 2022). Furthermore, recent studies have found that the bulk-Richardson number (Ri_b), in which local gradients present in Ri are approximated as bulk gradients, is sometimes better than MOST for parameterizing near-surface temperature, moisture, wind gradients (Lee and Buban 2020), as well as u_*, sensible heat flux (H), and latent heat flux (E) (Lee et al. 2021). For this reason, in the present study, we extended the studies by Lee and Buban (2020) and Lee et al. (2021) by developing Ri_b parameterizations for σ_u, σ_v, σ_w, σ_θ, and σ_q and comparing these parameterizations against parameterizations that use a MOST-based scaling approach.

2. Datasets

To develop parameterizations for $\sigma_{u,v,w,\theta,q}$, we used datasets obtained from three 10-m micrometeorological towers that were deployed during the Land Atmosphere Feedback Experiment (LAFE) in northern Oklahoma in August 2017. LAFE used a unique suite of surface and boundary layer profiling systems coupled with numerical simulations to study land atmosphere feedback processes and to improve the representation of these processes in NWP models. We refer the reader to e.g., Wulfmeyer et al. (2018) for more details about the experimental design and LAFE's objectives.

The 10-m towers were installed along a 1.7-km line oriented southwest to northeast in an early-growth soybean field (tower 1), native grassland (tower 2), and mature soybean field (tower 3) and consisted of the same array of instruments at all towers to sample bulk quantities and turbulence statistics. The surface roughness length (z_0) was approximately 0.10, 0.11, and 0.07 m for towers 1, 2, and 3, respectively, and the canopy displacement heights (d) at towers 1, 2, and 3 were around 0.91, 0.75, and 0.96 m, respectively. Sensitivity tests in which we vary z_0 indicate that minor differences in the values used for z_0 do not have a significant impact on the results in this study.

Datasets obtained between 1 and 31 August 2017 were used in all analyses. All turbulence statistics were sampled at 3 m above ground level (AGL) and 10 m AGL and at a 10-Hz sampling frequency. We applied standard postprocessing techniques to the 10-Hz datasets, including the coordinate rotations described in e.g., Meyers (2001) and Lee et al. (2019), as well corrections for angle-of-attack errors described in Kochendorfer et al. (2012). The mean diurnal cycles for $\sigma_{u,v,w,\theta,q}$ over the August 2017 sampling period are shown in Fig. 1. These analyses indicated that σ_u, σ_v, and σ_w had similar agreement among the three sites. σ_u and σ_v ranged from ~0.4 m s^{-1} during the nighttime to around 1.2 m s^{-1} in the early-middle afternoon hours, whereas σ_w ranged from ~0.2 to 0.5 m s^{-1}. σ_θ and σ_q showed slightly more variability among the sites than σ_u, σ_v, and σ_w; daytime values of σ_θ were lower over the soybean crop, and values of σ_q were correspondingly larger. We also found a small σ_θ increase around sunset at all three sites. Not surprisingly, the σ_θ increase varied as a function of wind speed and was largest under weak wind conditions around sunset that are most conducive to the development of local near-surface temperature gradients.

To ensure that we had high-quality datasets with which to develop the parameterizations for $\sigma_{u,v,w,\theta,q}$, we applied additional filtering procedures to the 30-min values of $\sigma_{u,v,w,\theta,q}$, ζ, and Ri_b. The application of additional filtering procedures on the datasets prior to developing the parameterizations in the present study was necessary to mitigate localized effects on the measurements. The filtering procedures for the LAFE datasets were originally described in Lee and Buban (2020) and Lee et al. (2021) and are briefly summarized here. We first removed observations made when the wind direction had a northerly component (i.e., >270° or <90°) because Lee and Buban (2020) noted that the longest fetch at each of the

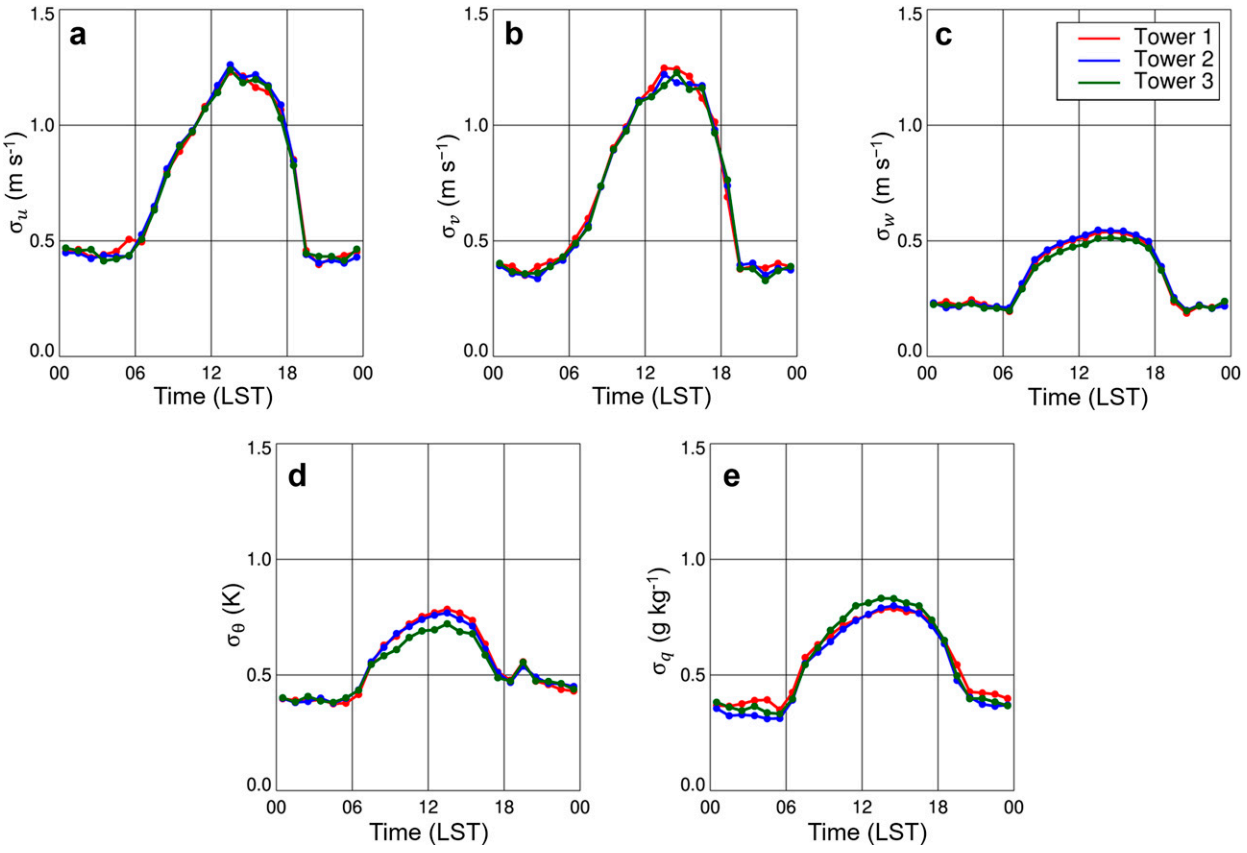

FIG. 1. Mean diurnal cycle of (a) σ_u, (b) σ_v, (c) σ_w, (d) σ_θ, and (e) σ_q as a function of time of day (LST = UTC − 6 h) at 10 m AGL at tower 1 (red line), tower 2 (blue line), and tower 3 (green line) averaged over 1–31 Aug 2017.

towers occurred when winds were from the south (i.e., Lee and Buban 2020). Doing so was particularly critical at tower 1 because the tower was installed near the boundary between an early-growth soybean field that extended approximately 210 m to the south of the tower and a mixed cropland north of the tower.

To further ensure high-quality, representative measurements we omitted 30-min averaging periods in which there was flux divergence occurring, as evident in the datasets by large differences in the fluxes at 3 and 10 m AGL (e.g., Lee et al. 2019, 2021). To this end, when developing the parameterizations for $\sigma_{u,v,w}$, we removed all 30-min periods when the percent difference in u_* between 3 and 10 m AGL exceeded 15%. Furthermore, we removed all 30-min periods when the percent difference in H between 3 and 10 m AGL exceeded 15% when determining the parameterizations for σ_θ, and we removed all 30-min periods when the percent difference in E between 3 and 10 m AGL exceeded 15% when determining the parameterizations for σ_q.

3. Derivation of parameterizations of turbulence statistics

a. ζ parameterizations

As there currently exists no widely accepted form for the relationship between $\sigma_{u,v,w,\theta,q}$ and ζ, we developed our own ζ-based parameterizations using the processed datasets from all three micrometeorological towers installed during LAFE. Doing so required that we first parameterize u_*. Following e.g., Lee et al. (2021), we compute u_* as

$$u_* = \frac{\kappa U}{\left[\ln\left(\frac{z-d}{z_0}\right) - \psi_m\left(\frac{z-d}{L}\right) + \psi_m\left(\frac{z_0}{L}\right)\right]}. \tag{6}$$

In Eq. (6), U is the wind speed which was sampled 10 m AGL, z is the sampling height, and the remaining variables have been defined previously. The integrated momentum similarity function ψ_m varies as a function of stability (e.g., Jiménez et al. 2012):

$$\psi_m = \begin{cases} 2\ln\left\{\frac{1+[\phi_m(\zeta)]^{-1}}{2}\right\} + \ln\left\{\frac{1+[\phi_m(\zeta)]^{-2}}{2}\right\} - 2\tan^{-1}\phi_m^{-1} + \frac{\pi}{2}, & \zeta < 0 \\ -\varepsilon_m\phi_m(\zeta), & \zeta > 0 \end{cases}. \tag{7}$$

In Eq. (7), we computed ϕ_m using Eq. (8), where the coefficients in Eq. (8) are those that Lee et al. (2021) determined using the LAFE datasets:

$$\phi_m = \begin{cases} 1.57(1 - 6.71\zeta)^{-0.25}, & \zeta < 0 \\ 4.04\zeta + 1.50, & \zeta > 0 \end{cases}. \tag{8}$$

To parameterize σ_θ and σ_q, we first used Eq. (6) to parameterize u_* and used the parameterized values for u_* in the equations below to derive H and E:

$$H = -\frac{\kappa \Delta\theta u_* c_p \rho}{\left[\ln\left(\frac{z_2 - d}{z_1 - d}\right) - \psi_h\left(\frac{z_2 - d}{L}\right) + \psi_h\left(\frac{z_1 - d}{L}\right)\right]}, \tag{9a}$$

$$E = -\frac{\kappa \Delta q u_* \rho L_v}{\left[\ln\left(\frac{z_2 - d}{z_1 - d}\right) - \psi_q\left(\frac{z_2 - d}{L}\right) + \psi_q\left(\frac{z_1 - d}{L}\right)\right]}. \tag{9b}$$

In Eq. (9), c_p is the specific heat capacity of air; ρ is the air density; $\Delta\theta$ is the near-surface potential temperature gradient, which was sampled between 10 m AGL (i.e., z_2) and 2 m AGL (i.e., z_1); Δq is the near-surface specific humidity gradient, which was sampled between 10 and 3 m AGL; L_v is the latent heat of vaporization; and ψ_h and ψ_q are the integrated similarity functions for heat and moisture, respectively, that were obtained from Lee et al. (2021). As is the case for ψ_m, both ψ_h and ψ_q vary as a function of atmospheric stability and have the following relationship:

$$\psi_{h,q} = \begin{cases} 2\ln\left\{\frac{1 + [\phi_{h,q}(\zeta)]^{-2}}{2}\right\}, & \zeta < 0 \\ -\varepsilon_{h,q}\phi_{h,q}(\zeta), & \zeta > 0 \end{cases}. \tag{10}$$

In the above equation, we computed ϕ_h using Eq. (11), where the coefficients are those that Lee et al. (2021) determined using the LAFE datasets:

$$\phi_h = \begin{cases} 1.06(1 - 1.10\zeta)^{-0.5}, & \zeta < 0 \\ 10.90\zeta + 1.05, & \zeta > 0 \end{cases}. \tag{11}$$

Similarily, we computed ϕ_q using Eq. (12), again where the coefficients in Eq. (12) were obtained by Lee et al. (2021):

$$\phi_q = \begin{cases} 1.15(1 - 5.15\zeta)^{-0.5}, & \zeta < 0 \\ 5.51\zeta + 1.64, & \zeta > 0 \end{cases}. \tag{12}$$

Once we parameterized u_*, H, and E, we performed nonlinear least squares regressions to relate the nondimensionalized forms of the turbulence statistics (i.e., by dividing $\sigma_{u,v,w}$ by u_* and dividing σ_θ and σ_q by θ_* and q_*, respectively) to ζ. θ_* and q_* are the temperature and moisture scales, respectively, and are computed following Eq. (13):

$$\theta_* = -\frac{\overline{w'\theta'}}{u_*}, \tag{13a}$$

$$q_* = -\frac{\overline{w'q'}}{u_*}. \tag{13b}$$

In the above equations, $\overline{w'\theta'}$ and $\overline{w'q'}$ are the kinematic forms of the heat and moisture flux, respectively.

For unstable conditions, we found that a 1/3 power law best fit the data for $\sigma_{u,v,w}/u_*$, whereas a −1/3 power-law best fit the data for σ_θ/θ_* and σ_q/q_*:

$$\frac{\sigma_{u,v,w}}{u_*} = \alpha_{\sigma_{u,v,w}}(1 - \beta_{\sigma_{u,v,w}}\zeta)^{1/3}, \tag{14a}$$

$$\frac{\sigma_\theta}{\theta_*} = \alpha_{\sigma_\theta}(1 - \beta_{\sigma_\theta}\zeta)^{-1/3}, \tag{14b}$$

$$\frac{\sigma_q}{q_*} = \alpha_{\sigma_q}(1 - \beta_{\sigma_q}\zeta)^{-1/3}. \tag{14c}$$

For stable conditions, the relationships have the following form:

$$\frac{\sigma_{u,v,w}}{u_*} = \mu_{\sigma_{u,v,w}}\exp(\nu_{\sigma_{u,v,w}}\zeta), \tag{15a}$$

$$\frac{\sigma_\theta}{\theta_*} = \mu_{\sigma_\theta}\exp(\nu_{\sigma_\theta}\zeta), \tag{15b}$$

$$\frac{\sigma_q}{q_*} = \mu_{\sigma_q}\exp(\nu_{\sigma_q}\zeta). \tag{15c}$$

In Eqs. (14) and (15), $\alpha_{\sigma_{u,v,w,\theta,q}}$, $\beta_{\sigma_{u,v,w,\theta,q}}$, $\mu_{\sigma_{u,v,w,\theta,q}}$, and $\nu_{\sigma_{u,v,w,\theta,q}}$ are empirically determined fitting coefficients. To determine these coefficients, we first computed the 1-sigma uncertainties in each observation. We then performed a Levenberg–Marquardt least squares fit which, using the observations and uncertainty within each observation, iteratively searches for the fitting coefficients until the chi-squared values are minimized. To determine the uncertainties in the observations, we used the approach described by e.g., Markowski et al. (2019) and Lee et al. (2021). To this end, the uncertainty in $\sigma_{u,v,w}/u_*$, i.e., $\delta(\sigma_{u,v,w}/u_*)$, is calculated as

$$\begin{aligned}\delta\left(\frac{\sigma_{u,v,w}}{u_*}\right) &= \left[\left(\frac{\partial\sigma_{u,v,w}u_*^{-1}}{\partial\sigma_{u,v,w}}\delta\sigma_{u,v,w}\right)^2 + \left(\frac{\partial\sigma_{u,v,w}u_*^{-1}}{\partial u_*}\delta u_*\right)^2\right]^{0.5} \\ &= \left[\left(\frac{\delta\sigma_{u,v,w}}{u_*^2}\right)^2 + \left(\frac{\sigma_{u,v,w}\delta u_*}{u_*^2}\right)^2\right]^{0.5}.\end{aligned} \tag{16}$$

The uncertainty in σ_θ/θ_* and σ_q/q_*, i.e., $\delta(\sigma_\theta/\theta_*)$ and $\delta(\sigma_q/q_*)$, respectively, is computed the same way as we computed $\delta(\sigma_{u,v,w}/u_*)$:

TABLE 1. Best-fit parameters using nonlinear least squares for $\sigma_{u,v,w}/u_* = \alpha_{\sigma_{u,v,w}}(1-\beta_{\sigma_{u,v,w}}\zeta)^{1/3}$, $\sigma_\theta/\theta_* = \alpha_{\sigma_\theta}(1-\beta_{\sigma_\theta}\zeta)^{-1/3}$, and $\sigma_q/q_* = \alpha_{\sigma_q}(1-\beta_{\sigma_q}\zeta)^{-1/3}$ over the range $-2 < \zeta < 0$. Also shown is 1-sigma uncertainty in each parameter, r, p value, and number of samples (N).

Variable	α	α uncertainty	β	β uncertainty	r	p	N
σ_u/u_*	2.419	0.019	1.127	0.137	0.514	<0.01	735
σ_v/u_*	2.100	0.022	4.067	0.313	0.584	<0.01	735
σ_w/u_*	1.196	0.014	1.492	0.222	0.778	<0.01	735
σ_θ/θ_*	4.354	0.551	39.524	18.755	0.626	<0.01	651
σ_q/q_*	6.303	0.132	40.906	3.393	0.614	<0.01	699

TABLE 2. As in Table 1, but for $\sigma_{u,v,w}/u_* = \mu_{\sigma_{u,v,w}}\exp(\nu_{\sigma_{u,v,w}}\zeta)$, $\sigma_\theta/\theta_* = \mu_{\sigma_\theta}\exp(\nu_{\sigma_\theta})$, and $\sigma_q/q_* = \mu_{\sigma_q}\exp(\nu_{\sigma_q})$ over the range $0 < \zeta < 1$.

Variable	μ	μ uncertainty	ν	ν uncertainty	r	p	N
σ_u/u_*	2.452	0.031	0.009	0.078	0.231	<0.01	572
σ_v/u_*	1.887	0.027	0.274	0.086	0.276	<0.01	572
σ_w/u_*	1.259	0.022	0.252	0.100	0.179	<0.01	572
σ_θ/θ_*	7.009	0.505	−1.109	0.392	0.305	<0.01	416
σ_q/q_*	8.047	0.072	1.015	0.052	0.095	0.047	434

$$\delta\left(\frac{\sigma_\theta}{\theta_*}\right) = \left[\left(\frac{\delta\sigma_\theta}{\theta_*^2}\right)^2 + \left(\frac{\sigma_\theta\delta\theta_*}{\theta_*^2}\right)^2\right]^{0.5}, \tag{17a}$$

$$\delta\left(\frac{\sigma_q}{q_*}\right) = \left[\left(\frac{\delta\sigma_q}{q_*^2}\right)^2 + \left(\frac{\sigma_q\delta q_*}{q_*^2}\right)^2\right]^{0.5}. \tag{17b}$$

Once we determined $\alpha_{\sigma_{u,v,w,\theta,q}}$, $\beta_{\sigma_{u,v,w,\theta,q}}$, $\mu_{\sigma_{u,v,w,\theta,q}}$, and $\nu_{\sigma_{u,v,w,\theta,q}}$, we then combined the equation for the parameterized u_* computed using MOST with the above relationships to compute $\sigma_{u,v,w}$ as

$$\sigma_{u,v,w} = \begin{cases} \dfrac{\kappa U}{\left[\ln\left(\dfrac{z-d}{z_0}\right) - \psi_m\left(\dfrac{z-d}{L}\right) + \psi_m\left(\dfrac{z_0}{L}\right)\right]}\alpha_{\sigma_{u,v,w}}(1-\beta_{\sigma_{u,v,w}}\zeta)^{1/3}, & \zeta < 0 \\ \dfrac{\kappa U}{\left[\ln\left(\dfrac{z-d}{z_0}\right) - \psi_m\left(\dfrac{z-d}{L}\right) + \psi_m\left(\dfrac{z_0}{L}\right)\right]}\mu_{\sigma_{u,v,w}}\exp(\nu_{\sigma_{u,v,w}}\zeta), & \zeta > 0 \end{cases}. \tag{18}$$

As we do for $\sigma_{u,v,w}$ we compute σ_θ as

$$\sigma_\theta = \begin{cases} \dfrac{\kappa\Delta\theta}{\left[\ln\left(\dfrac{z_2-d}{z_1-d}\right) - \psi_h\left(\dfrac{z_2-d}{L}\right) + \psi_h\left(\dfrac{z_1-d}{L}\right)\right]}\alpha_{\sigma_\theta}(1-\beta_{\sigma_\theta}\zeta)^{-1/3}, & \zeta < 0 \\ \dfrac{\kappa\Delta\theta}{\left[\ln\left(\dfrac{z_2-d}{z_1-d}\right) - \psi_h\left(\dfrac{z_2-d}{L}\right) + \psi_h\left(\dfrac{z_1-d}{L}\right)\right]}\mu_{\sigma_\theta}\exp(\nu_{\sigma_\theta}\zeta), & \zeta > 0 \end{cases}. \tag{19}$$

Similarly, we compute σ_q as

$$\sigma_q = \begin{cases} \dfrac{\kappa\Delta q}{\left[\ln\left(\dfrac{z_2-d}{z_1-d}\right) - \psi_q\left(\dfrac{z_2-d}{L}\right) + \psi_q\left(\dfrac{z_1-d}{L}\right)\right]}\alpha_{\sigma_q}(1-\beta_{\sigma_q}\zeta)^{-1/3}, & \zeta < 0 \\ \dfrac{\kappa\Delta q}{\left[\ln\left(\dfrac{z_2-d}{z_1-d}\right) - \psi_q\left(\dfrac{z_2-d}{L}\right) + \psi_q\left(\dfrac{z_1-d}{L}\right)\right]}\mu_{\sigma_q}\exp(\nu_{\sigma_q}\zeta), & \zeta > 0 \end{cases}. \tag{20}$$

The values for $\alpha_{\sigma_{u,v,w,\theta,q}}$, $\beta_{\sigma_{u,v,w,\theta,q}}$, $\mu_{\sigma_{u,v,w,\theta,q}}$, and $\nu_{\sigma_{u,v,w,\theta,q}}$ for $\zeta < 0$ and $\zeta > 0$ are shown in Tables 1 and 2, respectively, along with the 1-sigma errors in each fitting parameter.

b. Ri_b parameterizations

We again used the processed datasets from all three micrometeorological towers to compute the Ri_b. In the Ri_b approach,

which was described in e.g., Lee and Buban (2020) and Lee et al. (2021), local gradients present in the equation for the Richardson number are approximated as bulk gradients (e.g., Stull 1988):

$$\mathrm{Ri} = \frac{g\dfrac{\partial\overline{\theta_v}}{\partial z}}{\overline{\theta_v}\left[\left(\dfrac{\partial\overline{u}}{\partial z}\right)^2 + \left(\dfrac{\partial\overline{v}}{\partial z}\right)^2\right]} \approx \frac{g\Delta\overline{\theta_v}\Delta z}{\overline{\theta_v}[(\Delta\overline{u})^2 + (\Delta\overline{v})^2]} = \mathrm{Ri}_b. \quad (21)$$

Lee et al. (2021) then parameterized u_*, $\overline{w'\theta'}$, and $\overline{w'q'}$ as functions of the Ri_b:

$$u_* = UC_u(\mathrm{Ri}_b), \quad (22a)$$

$$\overline{w'\theta'} = -\Delta\theta u_* C_t(\mathrm{Ri}_b), \quad (22b)$$

$$\overline{w'q'} = -\Delta q u_* C_r(\mathrm{Ri}_b), \quad (22c)$$

For unstable conditions and stable conditions, i.e., when $\mathrm{Ri}_b < 0$ and $\mathrm{Ri}_b > 0$, respectively, $C_{u,t,r}$ has the following form:

$$C_{u,t,r} = \begin{cases} \lambda_{u,t,r}(1 - \omega_{u,t,r}\mathrm{Ri}_b)^{1/3}, & \mathrm{Ri}_b < 0 \\ \chi_{u,t,r}\exp(\gamma_{u,t,r}\mathrm{Ri}_b), & \mathrm{Ri}_b > 0 \end{cases}. \quad (23)$$

In the above equations, $\lambda_{u,t,r}$, $\omega_{u,t,r}$, $\chi_{u,t,r}$, and $\gamma_{u,t,r}$ are empirically determined fitting coefficients. As we did for the MOST parameterizations, we determined $\lambda_{u,t,r}$, $\omega_{u,t,r}$, $\chi_{u,t,r}$, and $\gamma_{u,t,r}$ using the Levenberg–Marquardt least squares fit described in section 3a. In this study, we used the same fitting coefficients as those found in Lee et al. (2021), which are reproduced in Table 3.

In Eq. (23), C_u, C_t, and C_r are the friction, heat-transfer, and moisture-transfer coefficients and are computed as

$$C_u = \frac{u_*}{U}, \quad (24a)$$

$$C_t = \frac{\theta_*}{\theta_v - \theta_{vs}}, \quad (24b)$$

$$C_r = \frac{q_*}{q - q_s}. \quad (24c)$$

In Eqs. (24a)–(24c), the subscript s denotes the surface values which, in the absence of temperature and moisture measurements directly at the land surface and following e.g., Seidel et al. (2012), Lee and Buban (2020), and Lee et al. (2021), we take to be the lowest sampling height on the tower which is 2-m AGL for θ_{vs} and 3 m AGL for q_s.

We found that a 1/3 power law best represented the relationship between $\sigma_{u,v,w}/u_*$ and Ri_b. Thus, for unstable conditions:

TABLE 3. Empirically determined fitting coefficients from Lee et al. (2021) used in Eq. (23).

Coefficient	Value
λ_u	0.08
λ_t	0.34
λ_r	0.18
ω_u	3.26
ω_t	10.34
ω_r	24.27
χ_u	0.08
χ_t	0.31
χ_r	0.15
γ_u	−3.11
γ_t	−9.25
γ_r	−13.59

$$\frac{\sigma_{u,v,w}}{u_*} = \lambda_{\sigma_{u,v,w}}(1 - \omega_{\sigma_{u,v,w}}\mathrm{Ri}_b)^{1/3}. \quad (25)$$

In contrast, we found that that a −1/3 power law best represented the relationship between σ_θ/θ_* and Ri_b, as well as between σ_q/q_* and Ri_b, when $\mathrm{Ri}_b < 0$. These relationships can be expressed following Eqs. (26a) and (26b), respectively:

$$\frac{\sigma_\theta}{\theta_*} = \lambda_{\sigma_\theta}(1 - \omega_{\sigma_\theta}\mathrm{Ri}_b)^{-1/3}, \quad (26a)$$

$$\frac{\sigma_q}{q_*} = \lambda_{\sigma_q}(1 - \omega_{\sigma_q}\mathrm{Ri}_b)^{-1/3}. \quad (26b)$$

Under stable conditions, we found that the functional forms of σ_u, σ_v, σ_w, σ_θ, and σ_q have the same relationship as the relationship between $C_{u,t,r}$ and Ri_b; thus $\sigma_{u,v,w}/u_*$, σ_θ/θ_*, and σ_q/q_* are computed as

$$\frac{\sigma_{u,v,w}}{u_*} = \chi_{\sigma_{u,v,w}}\exp(\gamma_{\sigma_{u,v,w}}\mathrm{Ri}_b), \quad (27a)$$

$$\frac{\sigma_\theta}{\theta_*} = \chi_{\sigma_\theta}\exp(\gamma_{\sigma_\theta}\mathrm{Ri}_b), \quad (27b)$$

$$\frac{\sigma_q}{q_*} = \chi_{\sigma_q}\exp(\gamma_{\sigma_q}\mathrm{Ri}_b). \quad (27c)$$

In the above equations, $\lambda_{\sigma_{u,v,w,\theta,q}}$, $\omega_{\sigma_{u,v,w,\theta,q}}$, $\chi_{\sigma_{u,v,w,\theta,q}}$, and $\gamma_{\sigma_{u,v,w,\theta,q}}$ are empirically determined from the LAFE datasets, again using the Levenberg–Marquardt least squares fit described in section 3a.

To compute $\sigma_{u,v,w}$, we combine the equation for the parameterized u_* derived using the Ri_b approach with the above relationships to compute $\sigma_{u,v,w}$ as

$$\sigma_{u,v,w} = \begin{cases} U\lambda_{u,v,w}(1 - \omega_{u,v,w}\mathrm{Ri}_b)^{1/3}\,\lambda_{\sigma_{u,v,w}}(1 - \omega_{\sigma_{u,v,w}}\mathrm{Ri}_b)^{1/3}, & \mathrm{Ri}_b < 0 \\ U\chi_{u,v,w}\exp(\gamma_{u,v,w}\mathrm{Ri}_b)\chi_{\sigma_{u,v,w}}\exp(\gamma_{\sigma_{u,v,w}}\mathrm{Ri}_b), & \mathrm{Ri}_b > 0 \end{cases}. \quad (28)$$

TABLE 4. Best-fit parameters using nonlinear least squares for $\sigma_{u,v,w}/u_* = \lambda_{\sigma_{u,v,w}}(1 - \omega_{\sigma_{u,v,w}}\mathrm{Ri}_b)^{1/3}$, $\sigma_\theta/\theta_* = \lambda_{\sigma_\theta}(1 - \omega_{\sigma_\theta}\mathrm{Ri}_b)^{-1/3}$, and $\sigma_q/q_* = \lambda_{\sigma_q}(1 - \omega_{\sigma_q}\mathrm{Ri}_b)^{-1/3}$ over the range $-2 < \mathrm{Ri}_b < 0$. Also shown is the 1-sigma uncertainty in each parameter, r, p value, and N.

Variable	λ	λ uncertainty	ω	ω uncertainty	r	p	N
σ_u/u_*	2.449	0.018	2.206	0.277	0.539	<0.01	696
σ_v/u_*	2.204	0.019	6.717	0.532	0.576	<0.01	696
σ_w/u_*	1.217	0.013	2.747	0.432	0.723	<0.01	696
σ_θ/θ_*	2.743	0.120	15.003	3.709	0.566	<0.01	440
σ_q/q_*	3.493	0.057	8.075	0.869	0.453	<0.01	362

As the parameterizations for σ_θ are a function of θ_* which itself is a function of the parameterized H, we can compute σ_θ as

$$\sigma_\theta = \begin{cases} \Delta\theta\lambda_t(1 - \omega_t\mathrm{Ri}_b)^{1/3}\,\lambda_{\sigma_\theta}(1 - \omega_{\sigma_\theta}\mathrm{Ri}_b)^{-1/3}, & \mathrm{Ri}_b < 0 \\ \Delta\theta\chi_t\exp(\gamma_t\mathrm{Ri}_b)\chi_{\sigma_\theta}\exp(\gamma_{\sigma_\theta}\mathrm{Ri}_b), & \mathrm{Ri}_b > 0 \end{cases}. \tag{29}$$

Similarly, the parameterizations for σ_q are a function of q_* which is a function of E; thus, we compute σ_q as

$$\sigma_q = \begin{cases} \Delta q\lambda_q(1 - \omega_q\mathrm{Ri}_b)^{1/3}\,\lambda_{\sigma_q}(1 - \omega_{\sigma_q}\mathrm{Ri}_b)^{-1/3}, & \mathrm{Ri}_b < 0 \\ \Delta q\chi_q\exp(\gamma_q\mathrm{Ri}_b)\chi_{\sigma_q}\exp(\gamma_{\sigma_q}\mathrm{Ri}_b), & \mathrm{Ri}_b > 0 \end{cases}. \tag{30}$$

The values for $\lambda_{\sigma_{u,v,w,\theta,q}}$, $\omega_{\sigma_{u,v,w,\theta,q}}$, $\chi_{\sigma_{u,v,w,\theta,q}}$, and $\gamma_{\sigma_{u,v,w,\theta,q}}$ for $\mathrm{Ri}_b < 0$ and $\mathrm{Ri}_b > 0$ are shown in Tables 4 and 5, respectively, along with the uncertainties in each fitting parameter. The values for r for the fits for σ_u/u_* and σ_v/u_* under unstable conditions are comparable between the MOST and Ri_b parameterizations; however, the values of r for the fits for the remaining variables are lower for the Ri_b parameterizations than for the MOST parameterizations. For stable regimes, both the MOST and Ri_b parameterizations have smaller values of r than for the unstable regimes. The fits for all variables except for σ_θ/θ_* have larger values of r for the Ri_b parameterizations. We suspect that the lower values of r for the fits arises due to the nonlinearity of the formulations themselves and to the small sample size.

4. Evaluation of ζ and Ri_b parameterizations for turbulence statistics

a. Datasets

We evaluated the ζ and Ri_b parameterizations of $\sigma_{u,v,w,\theta,q}$ using the observed 30-min $\sigma_{u,v,w,\theta,q}$ sampled 10 m AGL at all three LAFE micrometeorological towers. Unlike when developing the parameterizations, however, we did not filter the datasets by wind direction, nor did we remove periods when there were large differences in u_*, H, or E between 3 and 10 m AGL.

Additionally, we used a separate, fully independent dataset to evaluate the parameterizations. These datasets were obtained

TABLE 5. As in Table 4, but for the best-fit parameters for $\sigma_{u,v,w}/u_* = \chi_{\sigma_{u,v,w}}\exp(\gamma_{\sigma_{u,v,w}}\mathrm{Ri}_b)$, $\sigma_\theta/\theta_* = \chi_{\sigma_\theta}\exp(\gamma_{\sigma_\theta}\mathrm{Ri}_b)$, and $\sigma_q/q_* = \chi_{\sigma_q}\exp(\gamma_{\sigma_q}\mathrm{Ri}_b)$ over the range $0 < \mathrm{Ri}_b < 0.25$.

Variable	χ	χ uncertainty	γ	γ uncertainty	r	p	N
σ_u/u_*	2.435	0.033	0.494	0.327	0.512	<0.01	635
σ_v/u_*	1.894	0.029	1.383	0.359	0.473	<0.01	635
σ_w/u_*	1.331	0.024	−0.928	0.440	0.229	<0.01	633
σ_θ/θ_*	6.445	0.912	−3.949	2.879	0.130	0.032	273
σ_q/q_*	4.793	0.090	6.474	0.348	0.275	<0.01	176

from two 10-m micrometeorological towers that were installed to support the Verification of the Origins of Rotation in Tornadoes Experiment-Southeast (VORTEX-SE) campaign in northern Alabama. VORTEX-SE was a campaign focused on better understanding the surface and boundary layer processes that lead to severe weather genesis over the Southeast United States. We used datasets from towers installed near Belle Mina, Alabama, and Cullman, Alabama. The land surface surrounding the tower near Belle Mina consisted of grazed pasture, whereas the land surface surrounding the tower at Cullman was ungrazed grassland. Belle Mina and Cullman had values of z_0 of around 0.15 and 0.25 m, respectively, and d of about 0.4 and 1.1 m, respectively. More details about the VORTEX-SE experimental design and the sites themselves appear in, e.g., Lee et al. (2019) and Wagner et al. (2019).

We used the entire period of record from both towers (February 2016–April 2017), and we used 10-m observations of $\sigma_{u,v,w,\theta,q}$, again computed over 30 min and based on measurements sampled at 10 Hz, to evaluate the ζ and Ri_b parameterizations that we developed in the present study. The measurement suite at the towers at Belle Mina and Cullman was identical to the measurement suite at each of the LAFE towers, and we used the same data processing techniques for the high-frequency measurements as we did for the LAFE measurements. Following our approach for using the LAFE datasets to evaluate the ζ and Ri_b parameterizations, we did not apply any filtering criteria to either the Belle Mina or Cullman observations of $\sigma_{u,v,w,\theta,q}$ when evaluating the ζ and Ri_b parameterizations.

b. Weighting technique to evaluate ζ and Ri_b parameterizations

We followed the procedures described in Lee et al. (2021) to weight the errors from the observed $\sigma_{u,v,w,\theta,q}$ and parameterized $\sigma_{u,v,w,\theta,q}$. We then used the uncertainties in the observations and the uncertainties in the parameterized values as inputs into the following equations (Neri et al. 1989; Cantrell 2008; Lee et al. 2021):

$$W_i = \frac{w_{xi}w_{yi}}{w_{xi} + w_{yi}S^2}, \tag{31a}$$

$$W_i = \frac{w_{xi}w_{yi}}{w_{xi} + w_{yi}m_b^2}, \tag{31b}$$

$$b = \frac{\sum W_i(y_i - m_b x_i)}{\sum W_i}. \tag{31c}$$

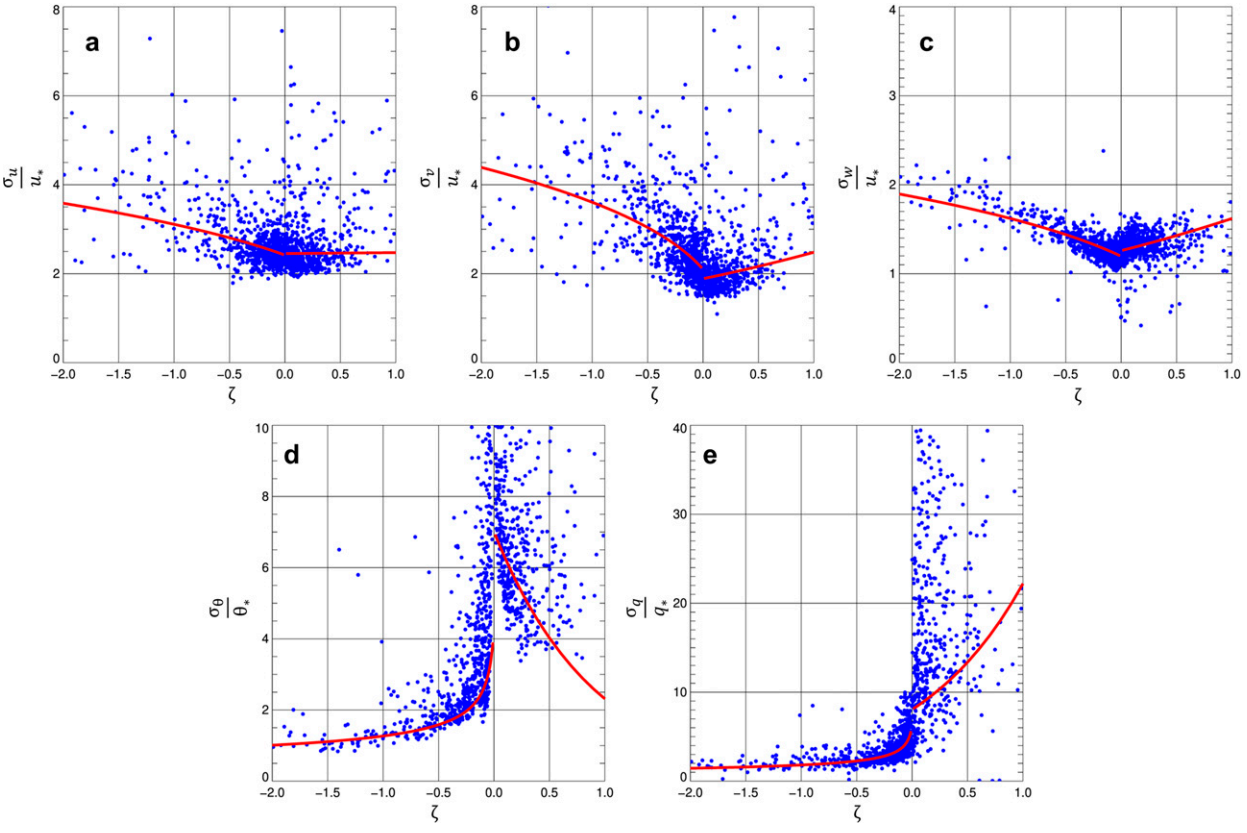

FIG. 2. (a) σ_u/u_*, (b) σ_v/u_*, (c) σ_w/u_*, (d) σ_θ/θ_*, and (e) σ_q/q_* as a function of ζ. Red line shows the line of best fit.

In Eqs. (31a)–(31c), x_i and y_i correspond with the observed $\sigma_{u,v,w,\theta,q}$ and parameterized $\sigma_{u,v,w,\theta,q}$, respectively; m_b is the slope of the fit; and w_{xi} and w_{yi} are the weights in the observations of $\sigma_{u,v,w,\theta,q}$ and parameterized values of $\sigma_{u,v,w,\theta,q}$, respectively. The equations were then solved iteratively until values for m_b and b were found that satisfied Eq. (31c).

5. Results and discussion

a. *Relationship between $\sigma_{u,v,w,\theta,q}$, ζ, and Ri_b*

Once the uncertainties in the each of the variables were computed using the approach described in section 3b, we were able to develop the relationships between $\sigma_{u,v,w,\theta,q}$ and ζ, as well as between $\sigma_{u,v,w,\theta,q}$ and Ri_b that weighted the observations as a function of the uncertainty in each measurement (Figs. 2 and 3). As noted in Tables 1 and 4 and briefly summarized here, when developing the MOST and Ri_b parameterizations, we used the same range for ζ for Ri_b for unstable conditions, i.e., $-2 < \zeta < 0$ and $-2 < Ri_b < 0$, respectively. As noted in Tables 2 and 5, though, we used a different range of stabilities for ζ for Ri_b for stable conditions, i.e., $0 < \zeta < 1$ and $0 < Ri_b < 0.25$, respectively, because of the relatively small number of cases when $Ri_b > 0.25$ compared to cases when $\zeta > 0.25$ and to remove the effects of outliers on the fits.

Consistent with previous work (e.g., Lee and Buban 2020; Lee et al. 2021), the scatter in these relationships was larger for stable conditions than for unstable conditions, which resulted in lower coefficients of correlation (r) under stable conditions, both for the ζ-based parameterizations and Ri_b-based parameterizations (cf. Tables 1, 2, 4, and 5). Furthermore, the nonlinear least squares fits for $\sigma_{u,v,w}/u_*$ had a larger r than the fits for σ_θ/θ_* and σ_q/q_*. We also note the comparatively small number of data points used to generate the fits for stable conditions because of the filtering criteria applied to the LAFE datasets which removed many periods during the nighttime in which the difference in the sensible heat fluxes and latent heat fluxes between the two sampling heights was nontrivial.

Furthermore, the relationships that we obtained between $\sigma_{u,v,w}/u_*$ and ζ were consistent with previous work. For example, when $\zeta \approx 0$, σ_u/u_*, σ_v/u_*, and σ_w/u_* were around 2.4, 2, and 1.2, respectively, which are within the range of values reported from the literature (e.g., Panofsky and Dutton 1984; de Franceschi et al. 2009). In contrast, we found a discontinuity near 0 in the relationship between σ_θ/θ_* and ζ, as well as in the relationship between σ_q/q_* and ζ, that arose due to the scatter present in these fits, particularly for stable conditions when r was 0.31 and 0.10, respectively. Consequently, σ_θ/θ_* was around 4.3 for slightly unstable conditions, but was around 7 for slightly stable conditions, which are values that are near the maximum values reported in the literature (e.g., de Franceschi et al. 2009). σ_q/q_* was ≈6.3 and 8.0 for slightly

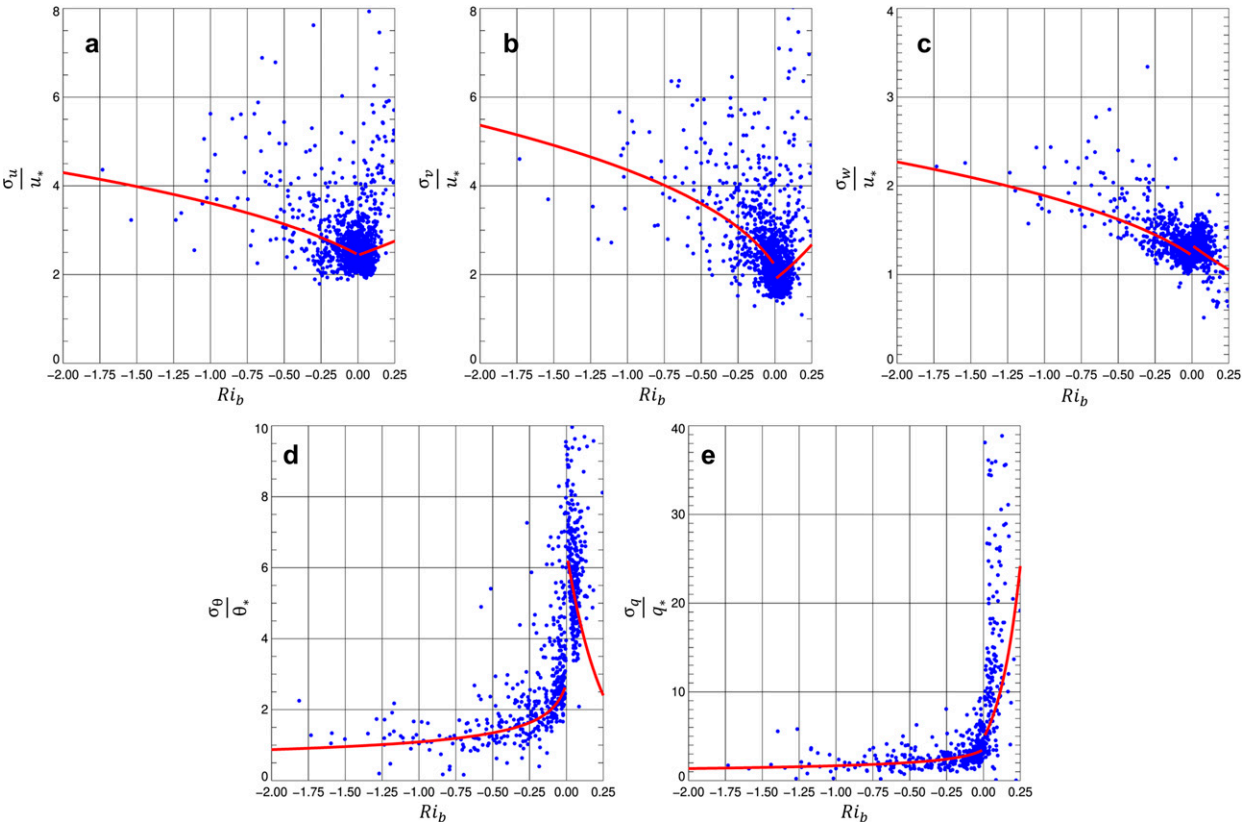

FIG. 3. (a) σ_u/u_*, (b) σ_v/u_*, (c) σ_w/u_*, (d) σ_θ/θ_*, and (e) σ_q/q_* as a function of Ri_b. Red line shows the line of best fit.

unstable conditions and slightly stable conditions, respectively. We acknowledge, though, that there are relatively few studies with which to compare our relationships between σ_q/q_* and ζ. However, we note that Quan and Hu (2009) found values of σ_q/q_* around 1.1 for near-neutral conditions, which were lower than the values we found using the LAFE datasets.

b. ζ and Ri_b parameterizations of $\sigma_{u,v,w}$

When we used the similarity relationships developed in the previous section to calculate $\sigma_{u,v,w}$, we found that the parameterized values of $\sigma_{u,v,w}$ were lower than the observed $\sigma_{u,v,w}$ when using the ζ parameterizations, not only the LAFE micrometeorological towers, but also at the VORTEX-SE micrometeorological towers. For example, m_b, which is the slope of the best-fit line between the observed and parameterized values and calculated after including the uncertainties in the observed and parameterized values following Eq. (31), was 0.80, 0.77, and 0.81 for σ_u, σ_v, and σ_w, respectively, at the LAFE towers (Figs. 4a–c). At Belle Mina, m_b was ~1 for σ_u, but was ~0.6 and ~0.8 for σ_v and σ_w, respectively (Figs. 4d–f). At Cullman, the correlation coefficients between the parameterized and observed $\sigma_{u,v,w}$ were comparable with Belle Mina (Figs. 4g–i), but m_b was lower at Cullman than at Belle Mina.

We found that the Ri_b parameterizations generally performed better than the ζ parameterizations, though this was not always the case. Whereas the values of r were comparable among the LAFE sites for the Ri_b and ζ parameterizations, m_b increased from 0.80 to 0.86, 0.77 to 0.82, and 0.81 to 0.99 for σ_u, σ_v, and σ_w, respectively (Figs. 5a–c). At Belle Mina, m_b increased for σ_u, σ_v, and σ_w; as a result the parameterizations overestimated these values (Figs. 5d–f). However, r increased from 0.62 to 0.68 and from 0.69 to 0.76 for σ_v, and σ_w, respectively. For σ_u, r decreased from 0.84 to 0.72 when using the Ri_b parameterizations instead of the ζ parameterizations at Belle Mina. At Cullman, the Ri_b parameterizations for σ_v performed better than the ζ parameterizations for σ_v, as m_b was closer to 1 and r was higher, but the Ri_b parameterizations did not perform as well as the ζ parameterizations for σ_u and σ_w based on these metrics (Figs. 5g–i).

c. ζ and Ri_b parameterizations of e

We used the parameterized σ_u, σ_v, and σ_w, computed using the MOST approach and the Ri_b approach, to parameterize turbulent kinetic energy, e, in the surface layer, and compared the parameterized e against the observed e which was computed as

$$e = 0.5(\sigma_u^2 + \sigma_v^2 + \sigma_w^2). \tag{32}$$

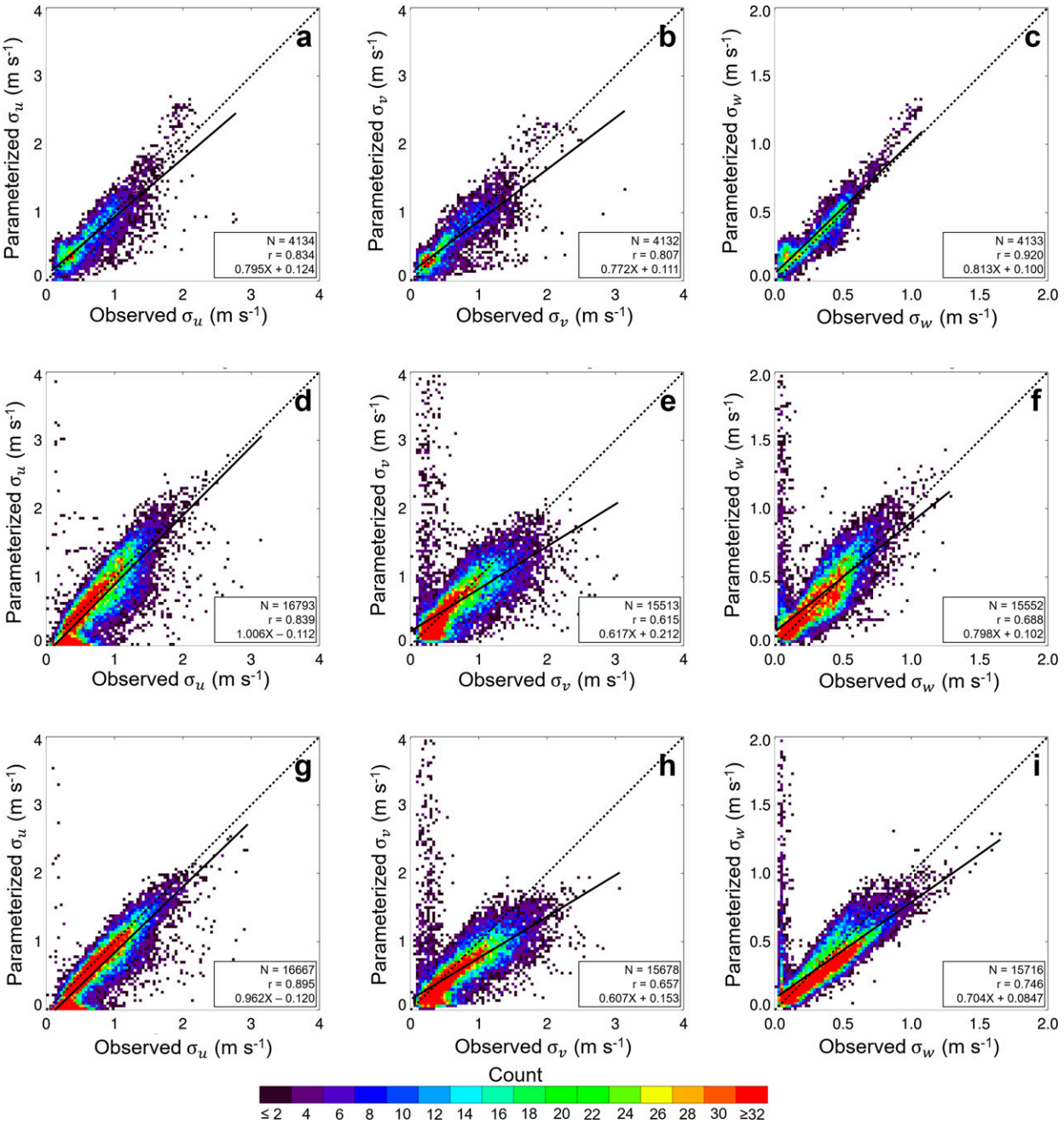

FIG. 4. (a) Density plot showing the relationship between the ζ-parameterized σ_u and observed σ_u for all three LAFE towers combined. (b),(c) As in (a), but for σ_v and σ_w, respectively. (d)–(f),(g)–(i) The relationships between the parameterized and observed σ_u, σ_v, and σ_w, respectively, at Belle Mina and Cullman, respectively. The dotted line shows the 1:1 line, and the solid line shows the line of best fit. N, r, and formula for the best-fit line (here, $X = m_b$) are shown at the bottom right of each panel.

As expected based on the relationships between the parameterized $\sigma_{u,v,w}$ and observed $\sigma_{u,v,w}$ in which the parameterizations underpredicted $\sigma_{u,v,w}$, both the ζ and Ri_b parameterizations also underpredicted e at the LAFE and VORTEX-SE micrometeorological towers (Fig. 6). At the LAFE towers, the ζ and Ri_b parameterizations performed similarly in their predictions of e. However, at Belle Mina, the Ri_b parameterizations performed better than the ζ parameterization based on the increase in m_b, as m_b was 0.87 and 0.77, for the Ri_b and ζ parameterizations, respectively. In contrast, the opposite occurred at Cullman, as m_b was 0.67 for the ζ parameterization of e but was 0.53 when we used the Ri_b parameterization.

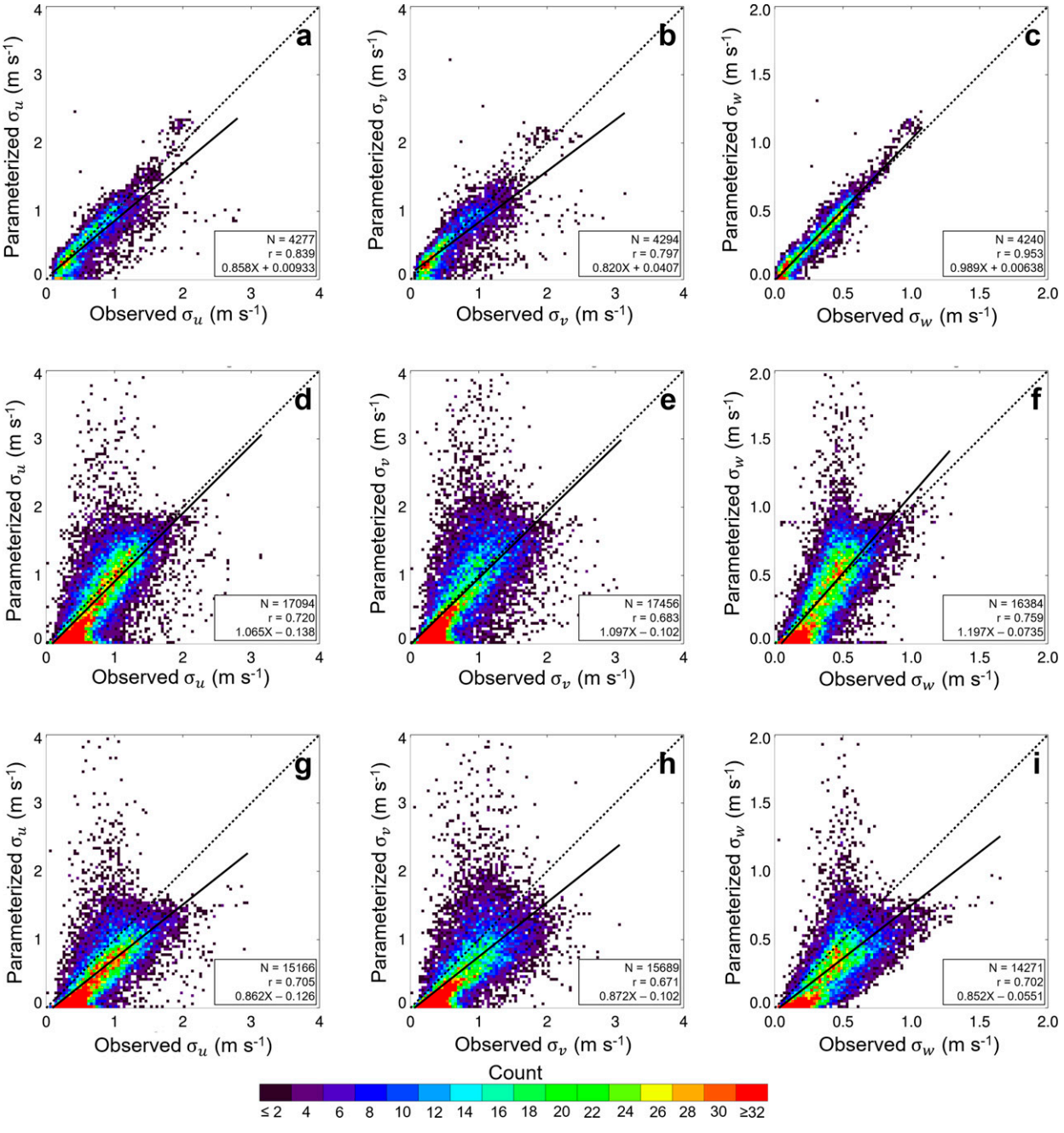

FIG. 5. As in Fig. 4, but for the Ri_b parameterizations.

d. ζ and Ri_b parameterizations of $\sigma_{\theta,q}$

When evaluating the relationships between the parameterized and observed values of $\sigma_{\theta,q}$ we found that the ζ parameterizations overpredicted σ_θ and σ_q at the LAFE towers; m_b was 1.04 and 1.17, respectively (Figs. 7a,b). At the VORTEX-SE towers, the opposite was true, and both m_b and r were considerably lower than at the LAFE towers. m_b for the relationship between the parameterized and observed σ_θ at Bella Mina and Cullman was 0.55 and 0.42, respectively; for σ_q, m_b was 0.24 and 0.91, respectively (Figs. 7c–f).

The Ri_b parameterizations generally yielded improved predictions for σ_θ and σ_q. At the LAFE towers, m_b was 0.85 and 0.92 for σ_θ and σ_q, respectively (Figs. 8a,b). At Belle Mina, there was marked improvement in m_b and r. m_b increased from 0.55 to 0.78 and 0.24 to 0.67 for σ_θ and σ_q, respectively, when using the Ri_b parameterizations instead of the ζ parameterizations;

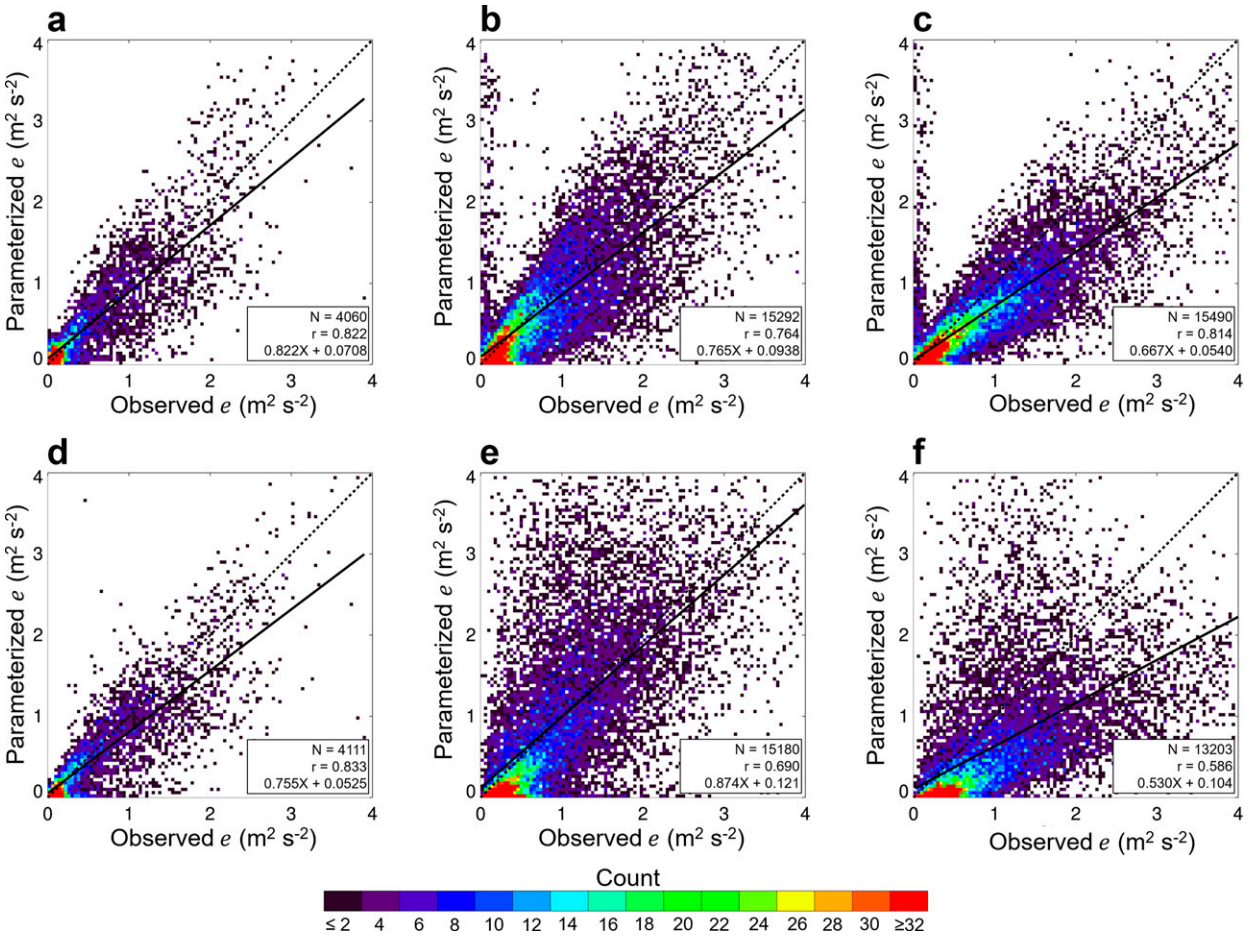

FIG. 6. Density plot showing the relationship between the ζ-parameterized e and observed e at (a) all three LAFE towers, (b) Belle Mina and (c) Cullman. (d)–(f) As in (a)–(c), but for the relationship between the Ri_b-parameterized e and observed e. The dotted line shows the 1:1 line, and the solid line shows the line of best fit. N, r, and formula for the best-fit line ($X = m_b$) are shown at the bottom right of each panel.

r increased from 0.43 to 0.64 and 0.07 to 0.45 for σ_θ and σ_q, respectively, when using the Ri_b parameterizations instead of the ζ parameterizations (Figs. 8c,d). We found similar increases in m_b and r when applying the Ri_b parameterizations to the Cullman datasets. m_b increased from 0.42 to 0.76 for σ_θ when using the Ri_b parameterizations instead of the ζ parameterizations, but the Ri_b parameterizations overestimated σ_q. However, r increased from 0.46 to 0.70 and 0.23 to 0.55 for σ_θ and σ_q, respectively (Figs. 8e,f).

Regardless, there is a nontrivial amount of scatter present in the relationship between the parameterized σ_q and observed σ_q, both in the ζ and Ri_b parameterizations, as r is typically smaller than the values found in the relationships for σ_θ. There are multiple reasons for the scatter between the parameterized and observed values. One of the reasons is that we did not filter either the LAFE or VORTEX-SE datasets by wind direction, nor did we remove periods when there were large differences in the fluxes at the two sampling heights, when evaluating the parameterizations not only for σ_θ and σ_q, but also when we evaluated the parameterizations of σ_u, σ_v, σ_w, and e. As expected, applying the same filtering criteria that we had used when developing the original parameterizations does reduce the scatter between the parameterized and observed turbulence statistics.

Overall, though, the σ_q parameterizations show the largest amount of scatter. Difficulties parameterizing near-surface moisture are well known. Lee and Buban (2020) and Lee et al. (2021) reported that parameterizations for Δq and E, respectively, in the surface layer yielded values that were at times significantly different from the observed values. As noted by Lee et al. (2021) and summarized here, the comparatively poor performance of moisture parameterizations in the surface layer, compared to parameterizations for surface-layer heat or momentum, can be attributed to advection and variability in landuse type, which are not represented in either the ζ or Ri_b parameterizations.

We also note much lower values of r at both Belle Mina and Cullman as compared with the values of r at the LAFE towers when evaluating the ζ and Ri_b parameterizations. This is true not only for σ_q but also for σ_θ. The poorer agreement

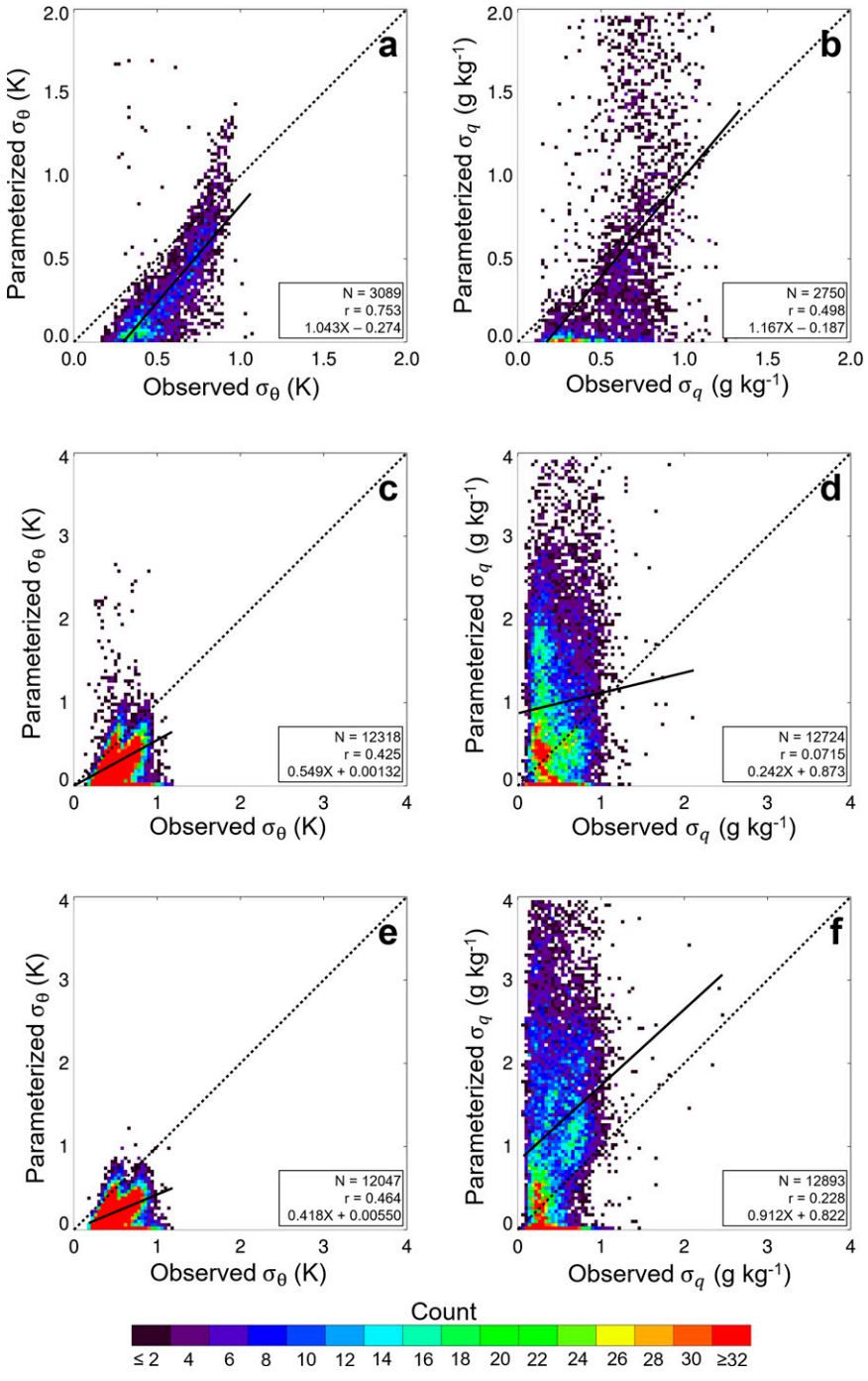

FIG. 7. (a) Density plot showing the relationship between the ζ-parameterized σ_θ and observed σ_θ at the LAFE towers. (b) As in (a), but for σ_q. (c),(d) The relationships between the parameterized and observed σ_θ and σ_q, respectively, at Belle Mina. (e),(f) As in (c) and (d), but for Cullman. The dotted line shows the 1:1 line, and the solid line shows the line of best fit. N, r, and formula for the best-fit line ($X = m_b$) are shown at the bottom right of each panel.

at Belle Mina and Cullman than at the LAFE sites arises because the parameterizations were developed over a semiarid region and then applied to a region in which E is a larger term in the surface energy budget.

e. *Performance of ζ and Ri_b parameterizations of $\sigma_{u,v,w,\theta,q}$ for different wind regimes*

Discussion so far has focused on the performance of the ζ and Ri_b parameterizations independent of wind speed.

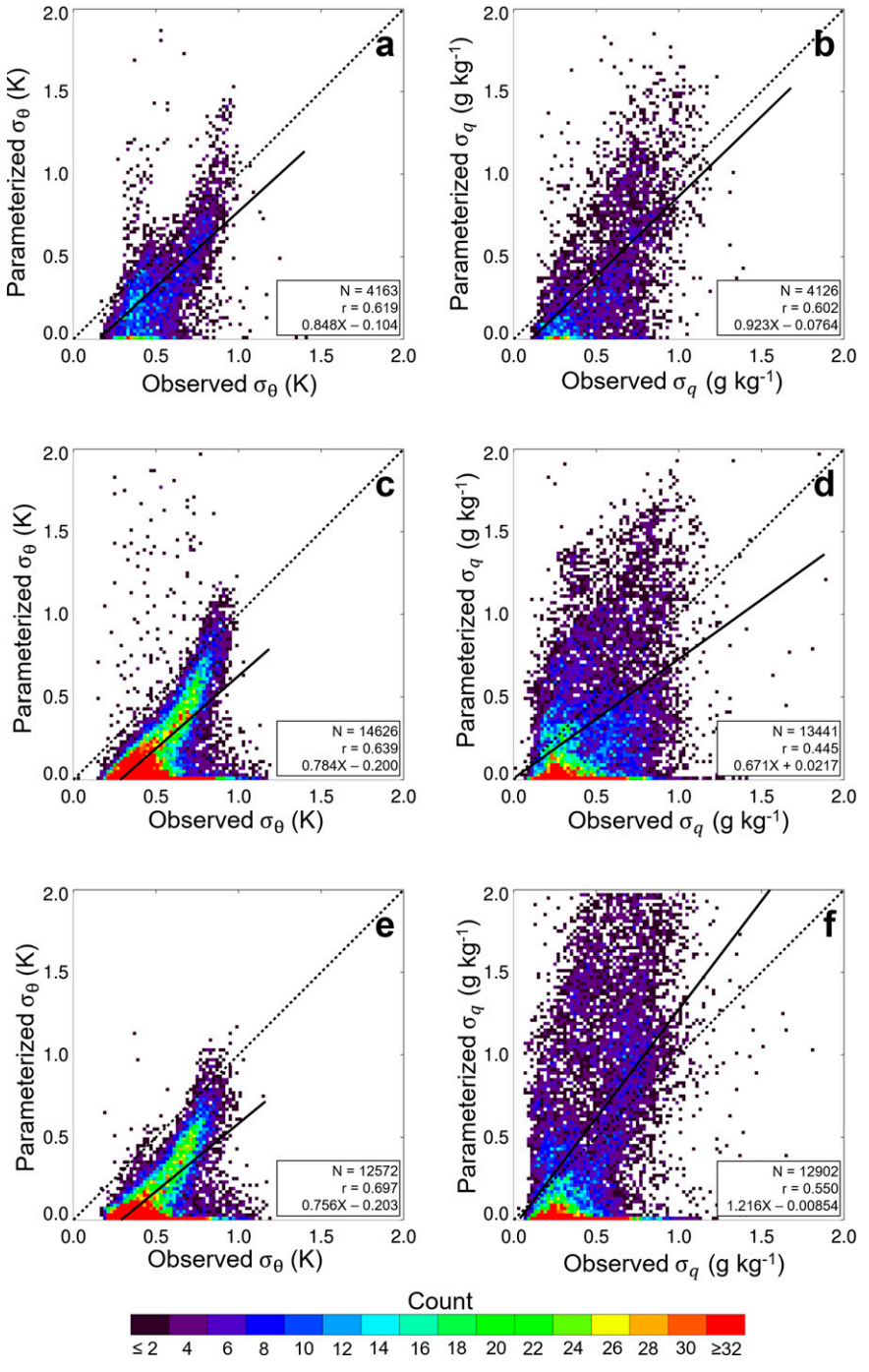

FIG. 8. As in Fig. 7, but for the Ri_b parameterizations.

However, recent work has shown that the Ri_b parameterizations generally perform better than the MOST parameterizations for low wind speeds (Lee et al. 2021). To this end, we distinguished between low wind speeds and high wind speeds by computing the median wind speed at the LAFE towers and at the Belle Mina and Cullman towers for the entire period of record at each site, which was 2.7, 2.0, and 2.5 m s^{-1}, respectively. We classified 30-min time periods with wind speeds below these thresholds as cases with low wind speeds, and we classified the 30-min periods with wind speeds above these thresholds as cases with high wind speeds.

The Ri_b parameterizations of σ_u, σ_v, and σ_w for the subset of cases with low wind speeds have larger r and m_b than the

TABLE 6. N, r, and formula for the best-fit line for the MOST and Ri_b parameterizations of $\sigma_{u,v,w}$, e, and $\sigma_{\theta,q}$ for low wind speeds at the LAFE towers and for the towers installed at Belle Mina and Cullman.

	σ_u	σ_v	σ_w	e	σ_θ	σ_q
			LAFE			
N						
MOST	2055	2053	2053	2053	1638	1438
Ri_b	2114	2130	2074	2021	1997	2025
r						
MOST	0.556	0.628	0.726	0.671	0.593	0.498
Ri_b	0.651	0.638	0.866	0.655	0.402	0.570
Best fit						
MOST	$0.313m_b + 0.248$	$0.406m_b + 0.177$	$0.422m_b + 0.131$	$0.300m_b + 0.103$	$0.654m_b - 0.127$	$0.839m_b - 0.124$
Ri_b	$0.562m_b + 0.0674$	$0.603m_b + 0.0635$	$0.821m_b + 0.0183$	$0.408m_b + 0.0437$	$0.524m_b + 0.0031$	$0.729m_b - 0.0439$
			Belle Mina			
N						
MOST	7161	5878	5912	5799	2838	3359
Ri_b	5854	6215	5114	4257	3644	3998
r						
MOST	0.524	0.0886	0.0491	0.132	0.511	0.0959
Ri_b	0.511	0.552	0.728	0.459	0.596	0.480
Best fit						
MOST	$0.462m_b - 0.0202$	$0.152m_b + 0.319$	$0.078m_b + 0.187$	$0.144m_b + 0.134$	$0.300m_b - 0.0033$	$0.310m_b + 0.786$
Ri_b	$1.018m_b - 0.146$	$1.257m_b - 0.181$	$1.379m_b - 0.0941$	$0.901m_b + 0.0626$	$0.481m_b - 0.124$	$0.610m_b - 0.0367$
			Cullman			
N						
MOST	10 363	9380	9411	9316	5755	6730
Ri_b	8626	9155	7730	6842	6055	6745
r						
MOST	0.727	0.284	0.332	0.379	0.559	0.156
Ri_b	0.577	0.617	0.697	0.519	0.700	0.564
Best fit						
MOST	$0.686m_b - 0.0459$	$0.336m_b + 0.224$	$0.379m_b + 0.130$	$0.289m_b + 0.111$	$0.286m_b + 0.0327$	$0.660m_b + 0.931$
Ri_b	$0.936m_b - 0.159$	$1.020m_b - 0.155$	$1.017m_b - 0.0833$	$0.799m_b - 0.009$	$0.631m_b - 0.177$	$1.247m_b - 0.078$

MOST parameterizations when evaluated using the LAFE datasets, whereas m_b is lower for the Ri_b parameterizations of σ_θ and σ_q (Table 6). At both Belle Mina and Cullman, m_b is better for the Ri_b parameterizations than for the MOST parameterizations for all turbulence statistics. Similar results are found for r; the only exception is that r is lower for the Ri_b parameterizations of σ_u than the MOST parameterizations at both sites.

Results are more mixed for the subset of cases with high wind speeds. The Ri_b parameterizations of σ_u and σ_v do not perform as well as the MOST parameterizations at the LAFE sites, whereas the performance is comparable for σ_w (Table 7). In the case of σ_θ, r is lower for the Ri_b parameterizations, but m_b is nearer to 1 than for the MOST parameterizations. The opposite is true for σ_q at the LAFE sites. At Belle Mina, m_b is nearer to 1 for all turbulence statistics for the Ri_b parameterizations than for the MOST parameterizations, yet r is lower when comparing the parameterized and observed values of σ_u, σ_v, σ_w and e. At Cullman, r and m_b are better for the Ri_b parameterizations of σ_θ and σ_q as compared with the MOST parameterizations.

6. Summary and outlook

Previous work found that using a Ri_b-based scaling approach works is comparable, if not better, than using a ζ-based scaling approach derived from MOST to compute near-surface gradients in wind, temperature, and moisture (Lee and Buban 2020) and fluxes of these respective quantities (Lee et al. 2021). Thus, in this work we developed parameterizations for σ_u, σ_v, σ_w, σ_θ, and σ_q that were a function of Ri_b and compared these parameterizations against techniques that use ζ as a scaling variable. To develop the ζ and Ri_b parameterizations, we used datasets from three 10-m micrometeorological towers installed during LAFE in August 2017. We evaluated the new parameterizations of turbulence statistics using not only the LAFE datasets but also by evaluating these parameterizations over a different region of the United States using fully independent datasets obtained from two 10-m micrometeorological towers installed during VORTEX-SE. Based on r and m_b, both of which are summarized in Fig. 9, between the Ri_b-parameterized quantities and observed turbulence statistics, we found that the Ri_b parameterizations better represented σ_v, σ_w, σ_θ, and σ_q than

TABLE 7. As in Table 6, but for high wind speeds.

	σ_u	σ_v	σ_w	e	σ_θ	σ_q
			LAFE			
N						
MOST	2067	2067	2068	1995	1446	1037
Ri_b	2150	2151	2153	2077	2153	2089
r						
MOST	0.824	0.794	0.938	0.813	0.819	0.299
Ri_b	0.801	0.769	0.948	0.820	0.712	0.556
Best fit						
MOST	$0.893m_b + 0.184$	$0.776m_b + 0.205$	$1.008m_b + 0.0505$	$0.843m_b + 0.192$	$1.299m_b - 0.382$	$0.980m_b + 0.0528$
Ri_b	$0.735m_b + 0.208$	$0.709m_b + 0.215$	$0.993m_b + 0.022$	$0.736m_b + 0.174$	$1.021m_b - 0.157$	$0.967m_b - 0.0430$
			Belle Mina			
N						
MOST	9632	9635	9640	9493	9480	9365
Ri_b	11 240	11 241	11 240	10 923	10 982	9443
r						
MOST	0.779	0.740	0.793	0.756	0.447	0.0612
Ri_b	0.693	0.657	0.707	0.676	0.670	0.442
Best fit						
MOST	$0.811m_b + 0.167$	$0.586m_b + 0.294$	$0.845m_b + 0.106$	$0.734m_b + 0.208$	$0.614m_b + 0.0064$	$0.213m_b + 0.906$
Ri_b	$0.984m_b - 0.0468$	$0.956m_b + 0.0296$	$1.145m_b - 0.0583$	$0.847m_b + 0.168$	$0.876m_b - 0.224$	$0.644m_b + 0.0652$
			Cullman			
N						
MOST	6304	6298	6305	6174	6292	6163
Ri_b	3540	6534	6541	6361	6517	6157
r						
MOST	0.819	0.699	0.738	0.761	0.507	0.318
Ri_b	0.574	0.554	0.508	0.519	0.717	0.525
Best fit						
MOST	$0.716m_b + 0.250$	$0.471m_b + 0.398$	$0.586m_b + 0.194$	$0.600m_b + 0.279$	$0.541m_b - 0.0223$	$1.197m_b + 0.692$
Ri_b	$0.664m_b + 0.0856$	$0.661m_b + 0.0970$	$0.587m_b + 0.0791$	$0.461m_b + 0.195$	$0.865m_b - 0.227$	$1.109m_b + 0.0988$

the MOST parameterizations, and the most significant improvements were for the Ri_b parameterizations of σ_θ and σ_q. Furthermore, the Ri_b parameterizations performed better than the MOST parameterizations under low wind speeds.

One important caveat about the Ri_b parameterizations that was described in Lee et al. (2021) and that also applies in the present study is that the Ri_b parameterizations use a stability term (i.e., Ri_b) which is closely related to the stability term used in MOST [i.e., L; cf. Eqs. (1), (2), and (21)], to represent surface-layer turbulence quantities. Thus, the Ri_b parameterizations are simply a different approach to represent surface layer physics through the use of a different term for near-surface stability; there is nothing inherently new about the Ri_b parameterizations of the underlying physics. Additionally, both the MOST and Ri_b parameterizations have self-correlation present. Self-correlation arises in the friction velocity term and the wind gradients in the MOST parameterizations and Ri_b parameterizations, respectively. However, the advantage of the Ri_b parameterizations is that bulk gradients are easier to measure than friction velocities (e.g., Lee et al. 2021). Furthermore, the Monin–Obukhov length scale in the MOST equations [cf. Eq. (2)] is a function of u_*^3. Thus, errors in the measured u_* can have a nontrivial impact on the Monin–Obukhov length scale (e.g., Markowski et al. 2019).

Overall, the results in this study, coupled with earlier studies arguing the need to revise MOST (e.g., Wilson 2008) and work by Lee and Buban (2020) and Lee et al. (2021), provide additional evidence that the functional forms of the similarity equations used in surface layer parameterization schemes within NWP models should be revisited and may need to be revised to use an Ri_b-based approach. Moving toward implementing an Ri_b-based approach in NWP models, however, requires that the newly suggested Ri_b parameterizations are evaluated over different landuse types and across a range of climatic conditions and atmospheric stability regimes (i.e., very unstable and very stable regimes) than has been so far been done (e.g., Olson et al. 2021). Furthermore, the newly suggested Ri_b parameterizations must be tested in large-eddy simulations, whereby not only are the parameterizations that we suggest in this study are tested but also the parameterizations for u_*, H, and E from Lee et al. (2021) are evaluated within these modeling frameworks prior to the parameterizations being implemented into operational NWP models.

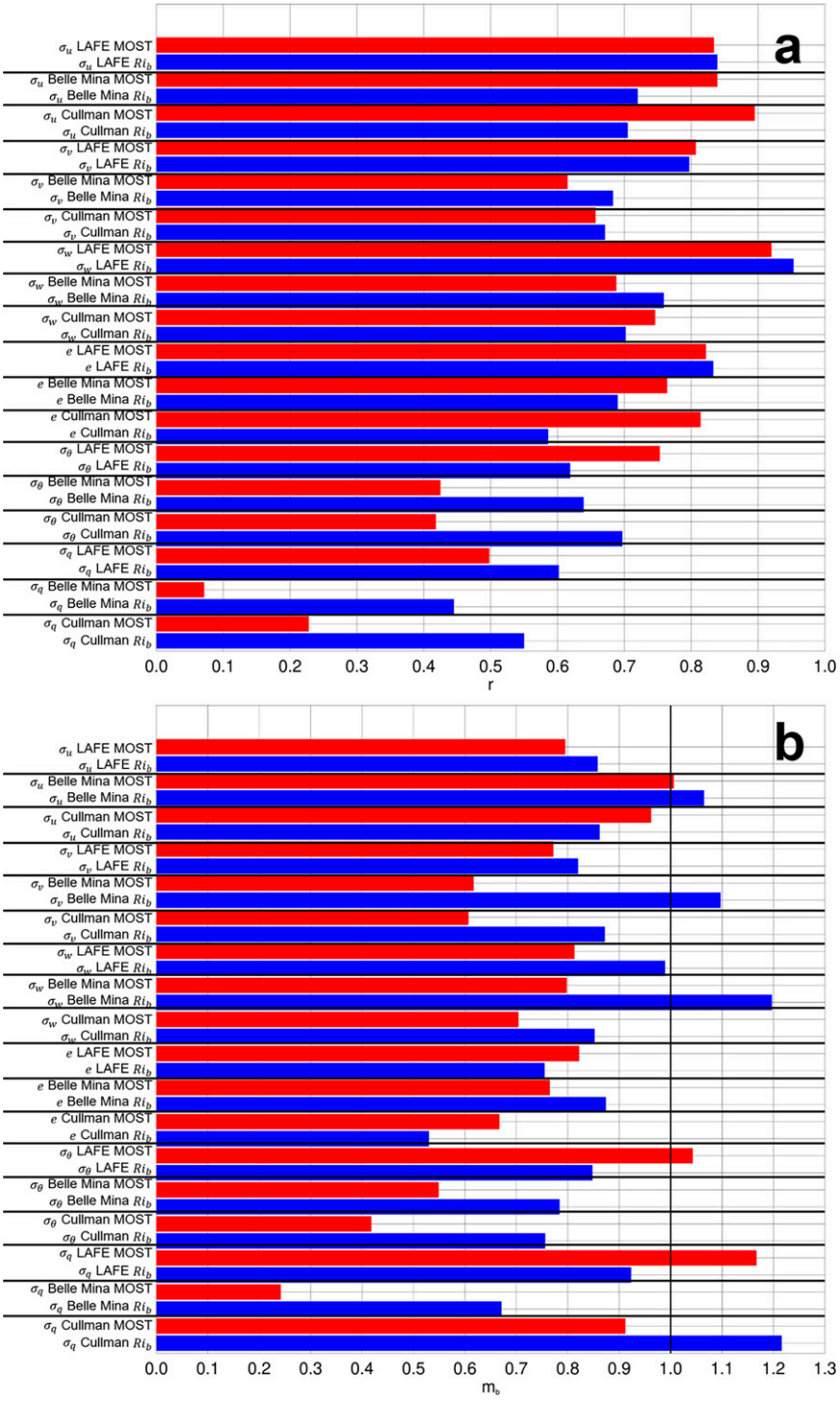

FIG. 9. Summary of (a) r and (b) m_b for the MOST (red bars) and Ri_b (blue bars) parameterizations of σ_u, σ_v, σ_w, e, σ_θ, and σ_q at the LAFE and VORTEX-SE towers. Horizontal black lines separate different variable–site combinations, and the vertical black line in (b) indicates a 1:1 relationship between the parameterized and observed turbulence statistics.

Acknowledgments. We thank Dr. David D. Turner of the NOAA/Earth Systems Research Laboratory Global Systems Laboratory and Dr. Volker Wulfmeyer of the University of Hohenheim for organizing LAFE, and we thank Dr. Michael Buban for useful discussions regarding this work. We thank Mr. Mark Heuer and Mr. Randy White from NOAA/ARL/ATDD for helping us to install and maintain the meteorological measurements installed on each tower during LAFE and VORTEX-SE. We acknowledge the three anonymous reviewers whose suggestions helped us to improve the manuscript. Finally, we note that the results and conclusions of this study, as well as any views expressed herein, are those of the authors and do not necessarily reflect those of NOAA or the Department of Commerce.

Data availability statement. The datasets from the three micrometeorological towers installed to support LAFE are available from https://www.arm.gov/research/campaigns/sgp2017lafenoaaarlatdd. The datasets from the micrometeorological towers installed to support VORTEX-SE and that were used to help evaluate the parameterizations of turbulence statistics developed in this study can be accessed at https://data.eol.ucar.edu/dataset/527.008 (for the 2016 VORTEX-SE campaign) and https://data.eol.ucar.edu/dataset/541.021 (for the 2017 VORTEX-SE campaign).

REFERENCES

Al-Jiboori, M. H., Y. Xu, and Y. Qian, 2002: Local similarity relationships in the urban boundary layer. *Bound.-Layer Meteor.*, **102**, 63–82, https://doi.org/10.1023/A:1012745322728.

Andreas, E. L., R. J. Hill, J. R. Gosz, D. I. Moore, W. D. Otto, and A. D. Sarma, 1998: Statistics of surface-layer turbulence over terrain with metre-scale heterogeneity. *Bound.-Layer Meteor.*, **86**, 379–408, https://doi.org/10.1023/A:1000609131683.

Businger, J. A., J. C. Wyngaard, Y. Izumi, and E. F. Bradley, 1971: Flux-profile relationships in the atmospheric surface layer. *J. Atmos. Sci.*, **28**, 181–189, https://doi.org/10.1175/1520-0469(1971)028<0181:FPRITA>2.0.CO;2.

Cantrell, C. A., 2008: Review of methods for linear least-squares fitting of data and application to atmospheric chemistry problems. *Atmos. Chem. Phys.*, **8**, 5477–5487, https://doi.org/10.5194/acp-8-5477-2008.

de Franceschi, M., D. Zardi, M. Tagliazucca, and F. Tampieri, 2009: Analysis of second-order moments in surface layer turbulence in an alpine valley. *Quart. J. Roy. Meteor. Soc.*, **135**, 1750–1765, https://doi.org/10.1002/qj.506.

Foken, T., 2006: 50 years of the Monin–Obukhov similarity theory. *Bound.-Layer Meteor.*, **119**, 431–447, https://doi.org/10.1007/s10546-006-9048-6.

Greene, B. R., S. T. Kral, P. B. Chilson, and J. Reuder, 2022: Gradient-based turbulence estimates from multicopter profiles in the Arctic stable boundary layer. *Bound.-Layer Meteor.*, **183**, 321–353, https://doi.org/10.1007/s10546-022-00693-x.

Hicks, B. B., 1978: Some limitations of dimensional analysis and power laws. *Bound.-Layer Meteor.*, **14**, 567–569, https://doi.org/10.1007/BF00121895.

——, 1981: An examination of turbulence statistics in the surface boundary layer. *Bound.-Layer Meteor.*, **21**, 389–402, https://doi.org/10.1007/BF00119281.

——, 1995: Monin–Obukhov similarity—An historical perspective. Preprints, *11th Symp. on Boundary Layers and Turbulence*, Charlotte, NC, Amer. Meteor. Soc., 1–4.

Jiménez, P. A., J. Dudhia, J. F. González-Rouco, J. Navarro, J. P. Montávez, and E. García-Bustamante, 2012: A revised scheme for the WRF surface layer formulation. *Mon. Wea. Rev.*, **140**, 898–918, https://doi.org/10.1175/MWR-D-11-00056.1.

Kochendorfer, J., T. P. Meyers, J. Frank, W. J. Massman, and M. W. Heuer, 2012: How well can we measure the vertical wind speed? Implications for fluxes of energy and mass. *Bound.-Layer Meteor.*, **145**, 383–398, https://doi.org/10.1007/s10546-012-9738-1.

Lee, T. R., and M. Buban, 2020: Evaluation of Monin–Obukhov and bulk Richardson parameterizations for surface–atmosphere exchange. *J. Appl. Meteor. Climatol.*, **59**, 1091–1107, https://doi.org/10.1175/JAMC-D-19-0057.1.

——, ——, D. D. Turner, T. P. Meyers, and C. B. Baker, 2019: Evaluation of the High-Resolution Rapid Refresh (HRRR) model using near-surface meteorological and flux observations from northern Alabama. *Wea. Forecasting*, **34**, 635–663, https://doi.org/10.1175/WAF-D-18-0184.1.

——, ——, and T. P. Meyers, 2021: Application of bulk Richardson parameterizations of surface fluxes to heterogeneous land surfaces. *Mon. Wea. Rev.*, **149**, 3243–3264, https://doi.org/10.1175/MWR-D-21-0047.1.

Markowski, P. M., N. T. Lis, D. D. Turner, T. R. Lee, and M. S. Buban, 2019: Observations of near-surface vertical wind profiles and vertical momentum fluxes from VORTEX-Southeast 2017: Comparisons to Monin–Obukhov similarity theory. *Mon. Wea. Rev.*, **147**, 3811–3824, https://doi.org/10.1175/MWR-D-19-0091.1.

Mauritsen, T., G. Svensson, S. S. Zilitinkevich, I. Esau, L. Enger, and B. Grisogono, 2007: A total turbulent energy closure model for neutrally and stably stratified atmospheric boundary layers. *J. Atmos. Sci.*, **64**, 4113–4126, https://doi.org/10.1175/2007JAS2294.1.

Meyers, T. P., 2001: A comparison of summertime water and CO_2 fluxes over rangeland for well watered and drought conditions. *Agric. For. Meteor.*, **106**, 205–214, https://doi.org/10.1016/S0168-1923(00)00213-6.

Neri, F., G. Saitta, and S. Chiofalo, 1989: An accurate and straightforward approach to line regression analysis of error-affected experimental data. *J. Phys. E: Sci. Instrum.*, **22**, 215–217, https://doi.org/10.1088/0022-3735/22/4/002.

Olson, J. B., T. Smirnova, J. S. Kenyon, D. D. Turner, J. M. Brown, W. Zheng, and B. W. Green, 2021: A description of the MYNN surface-layer scheme. NOAA Tech. Memo. OAR GSL-67, 26 pp., https://doi.org/10.25923/f6a8-bc75.

Pahlow, M., M. B. Parlange, and F. Porté-Agel, 2001: On Monin–Obukhov similarity in the stable atmospheric boundary layer. *Bound.-Layer Meteor.*, **99**, 225–248, https://doi.org/10.1023/A:1018909000098.

Panofsky, H. A., and R. A. McCormick, 1960: The spectrum of vertical velocity near the surface. *Quart. J. Roy. Meteor. Soc.*, **86**, 495–503, https://doi.org/10.1002/qj.49708637006.

——, and J. A. Dutton, 1984: *Atmospheric Turbulence: Models and Methods for Engineering Applications*. John Wiley and Sons, 389 pp.

——, H. Tennekes, D. H. Lenschow, and J. C. Wyngaard, 1977: The characteristics of turbulent velocity components in the surface layer under convective conditions. *Bound.-Layer Meteor.*, **11**, 355–361, https://doi.org/10.1007/BF02186086.

Quan, L., and F. Hu, 2009: Relationship between turbulent flux and variance in the urban canopy. *Meteor. Atmos. Phys.*, **104**, 29–36, https://doi.org/10.1007/s00703-008-0012-5.

Ramana, M. V., P. Krishnan, and P. K. Kunhikrishnan, 2004: Surface boundary-layer characteristics over a tropical inland station: Seasonal features. *Bound.-Layer Meteor.*, **111**, 153–157, https://doi.org/10.1023/B:BOUN.0000010999.25921.1a.

Seidel, D. J., Y. Zhang, A. Beljaars, J.-C. Golaz, A. R. Jacobson, and B. Medeiros, 2012: Climatology of the planetary boundary layer over the continental United States and Europe. *J. Geophys. Res.*, **117**, D17106, https://doi.org/10.1029/2012JD018143.

Sorbjan, Z., 2006: Comments on 'Flux-gradient relationship, self-correlation and intermittency in the stable boundary layer.' *Quart. J. Roy. Meteor. Soc.*, **132**, 1371–1373, https://doi.org/10.1256/qj.05.168A.

——, 2010: Gradient-based scales and similarity laws in the stable boundary layer. *Quart. J. Roy. Meteor. Soc.*, **136**, 1243–1254, https://doi.org/10.1002/qj.638.

——, 2017: Assessment of gradient-based similarity functions in the stable boundary layer derived from a large-eddy simulation. *Bound.-Layer Meteor.*, **163**, 375–392, https://doi.org/10.1007/s10546-017-0234-5.

Srivastava, P., M. Sharan, and M. Kumar, 2020: Development of observation-based parameterisations of standard deviation of wind velocity fluctuations over an Indian region. *Theor. Appl. Climatol.*, **139**, 1057–1077, https://doi.org/10.1007/s00704-019-02999-2.

Stull, R. B., 1988: *An Introduction to Boundary Layer Meteorology*. Kluwer Academic, 666 pp.

Sun, J., E. S. Takle, and O. C. Acevedo, 2020: Understanding physical processes represented by the Monin—Obukhov bulk formula for momentum transfer. *Bound.-Layer Meteor.*, **177**, 69–95, https://doi.org/10.1007/s10546-020-00546-5.

Wagner, T. J., P. M. Klein, and D. D. Turner, 2019: A new generation of ground-based mobile platforms for active and passive profiling of the boundary layer. *Bull. Amer. Meteor. Soc.*, **100**, 137–153, https://doi.org/10.1175/BAMS-D-17-0165.1.

Wilson, J. D., 2008: Monin-Obukhov functions for standard deviations of velocity. *Bound.-Layer Meteor.*, **129**, 353–369, https://doi.org/10.1007/s10546-008-9319-5.

Wulfmeyer, V., and Coauthors, 2018: A new research approach for observing and characterizing land–atmosphere feedback. *Bull. Amer. Meteor. Soc.*, **99**, 1639–1667, https://doi.org/10.1175/BAMS-D-17-0009.1.